Received: 12 August 2021 | Revised: 17 September 2021 | Accepted: 28 September 2021

DOI: 10.1002/agt2.132

Aggregate Open Access WILEY

REVIEW

Metal nanocluster-based devices: Challenges and opportunities

Nanoscience: Special Issue Dedicated to Professor Paul S. Weiss

Lizhen Chen[1] | **Andres Black**[2] | **Wolfgang J. Parak**[1] | **Christian Klinke**[3,4,5] | **Indranath Chakraborty**[1]

[1] Faculty of Physics, Center for Hybrid Nanostructures (CHyN), University Hamburg, Hamburg, Germany

[2] ICFO – Institut de Ciencies Fotoniques, The Barcelona Institute of Science and Technology, Barcelona, Spain

[3] Institute of Physics, University of Rostock, Rostock, Germany

[4] Department of Life, Light & Matter, University of Rostock, Rostock, Germany

[5] Department of Chemistry, Swansea University, Swansea, UK

Correspondence
Indranath Chakraborty, Faculty of Physics, Center for Hybrid Nanostructures (CHyN), University Hamburg, Hamburg, 22607, Germany.
Email: indranath.chakraborty@physik.uni-hamburg.de
Christian Klinke, Department of Chemistry, Swansea University, Singleton Park, Swansea SA2 8PP, UK.
Email: christian.klinke@uni-rostock.de

Funding information
Fonds der Chemischen Industrie im Verband der Chemischen Industrie; Deutsche Forschungsgemeinschaft, Grant/Award Number: EXC 2056-project ID 390715994; Chinese Scholarship Council

Abstract

Atomically precise nanoclusters (NCs) with fascinating physicochemical characteristics different from their nanoparticles (NPs) counterparts have gained increasing attention in diverse fields of applications. The foremost outcome of such NC-based applications is leading to transform them into devices. In fact, there are already some reports on the development of NC-based devices. For instance, NCs exhibit their potential in solar cells, showing high light-harvesting efficiency comparable to traditional semiconductor solar cells. Further, recent progress in characterizing Au NCs films and micro-crystals shows semiconductor-like properties such as field effect and photoresponse. These successes indicate that metal NCs possess a high potential for application in multidisciplinary areas for advancing the development in fundamental and practical purposes. However, no such comprehensive review is available to highlight recent advances and new applicable devices based on noble metal NCs. Herein, we reviewed the recent development in this area, including synthesis challenges of metal NCs and related applications of NC-sensitized solar cells, strain sensors, chemo-/biosensors, transistors, floating memory, and other devices. Furthermore, the future opportunities such as modifying synthetic methods to make other metal NCs, enhancing the efficiency of solar cells, and exploring more NC-based devices alternative to semiconductors are pointed out. We hope that rapidly increasing interest in NC-based devices will stimulate the research in this area and inspire the advances in combined devices accordingly.

KEYWORDS

memory devices, metal nanoclusters, sensors, solar cells, transistors

1 | INTRODUCTION

Nanoscience has witnessed immense advancements associated with metal nanoparticles (NPs) due to their interesting properties compared to their bulk counterparts.[1–3] Various metal NPs (especially noble metals such as Pt, Au, Ag) have been employed in the fields of biomedicine, sensors, catalysis, as well as photovoltaics.[4–8] Besides, advanced devices based on metal NPs have been immensely developed in the areas of fuel cells, analytical sensors, optoelectronic devices, etc.[9–12] For instance, solar cells, as renewable energy devices with numerous merits, such as low-cost, portability, environmental friendliness, as well as high energy efficiency, have been intensely studied and utilized to tackle the presently urgent energy crisis.[1,13–23] Moreover, taking advantage of the fast charge transfer rate from metal NPs to polymer layers, the design of metal NP-based floating memory devices exhibits promising potential.[24–26] Besides such a plethora of studies focused on NP-based applications, size-controlled nanoclusters (NCs), have become another fast-growing interest in nanomaterial science.[27–29] Metal NCs, consisting of a few to hundreds of atoms, have been intensively studied because of their unique physical and chemical properties, resulting from their molecule-like discrete energy levels.[30–35] These make NCs suitable candidates in various applications from sensing to photovoltaics.[8,36–40] Recently, metal NC-sensitized solar cells (MCSCs) have received an increasing attention as emerging photovoltaic devices, possessing similar structure compared to dye-sensitized solar cells (DSSCs).[36,41–43] NPs-based SCs presented limited enhancement in the power conversion efficiency (PCE) because of the possible energy transfer via nonradiative pathway as well as disturbance of the interface morphology.[44] Metal NPs possess surface plasmon resonance which covers only a certain portion of the visible light whereas most of the metal NCs has multiple bands covering a large

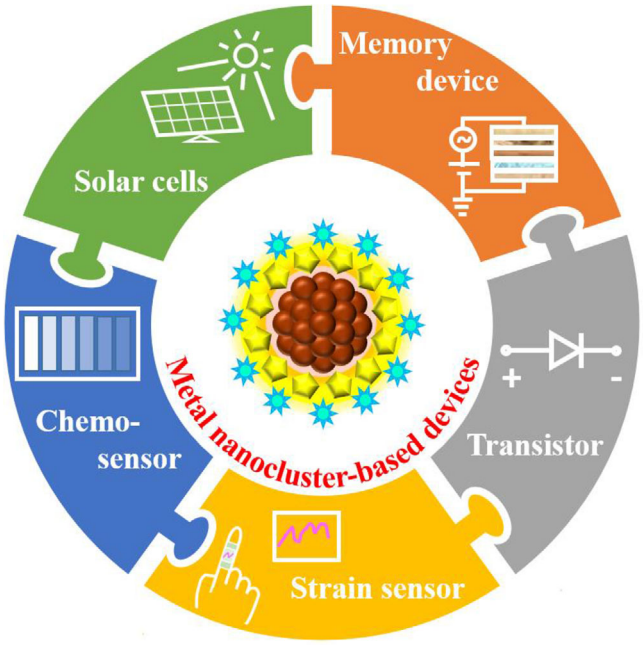

SCHEME 1 Illustration of metal NC-based devices classified by function

portion of the visible light facilitating the efficiency of solar cell.[45] Additionally, NCs exhibit photoluminescence, showing thus advantages over their plasmonic NPs counterparts in this regard.[46] Several reviews have been committed to metal NCs due to their distinct properties. Apart from the synthesis of NCs, most of them are focused on their applications as fluorescent probes, probes for diagnosis, as well as analytical sensing types of applications.[9,27,46] Recently a significant number of research articles have been reported on NC-based devices. This review attempts to summarize the present well-developed and applicable device by using metal NCs as platforms. In the first section of the review, typical synthetic challenges of NCs production will be pointed out. Then, subsequently, NC-based devices will be explained and classified by their function (Scheme 1), including solar cells, strain sensors, chemo- or biosensors, transistors, and floating memory as well as other devices. In the last section, a brief outlook will be provided on the current challenges and opportunities of metal NC-based devices for future research.

2 | SYNTHETIC CHALLENGES FOR METAL NCs

Even after the enormous growth in the synthesis protocols for NCs in the recent years, approaches for converting them to a device have not grown with the same speed. Purity and stability of NCs are two important issues that hamper their applications to make devices of improved performance. Purity is foremost important to achieve controlled electronic properties for carrying out electrical transport experiments on high-quality metal NCs films[47] and crystals.[48] NCs are atomically pure in most of the cases, but even after that there are plenty of other impurities that can drastically affect the device performance. For example, the presence of small, charged byproducts can contribute to electronic instability in the films and deviations from ideal behavior. These byproducts can act as scattering centers for charge carriers in the film, which results in an ionic current moving through the matrix of the film in response to applied electric fields. Consequently, these mobile, ion-like charges will tend to screen the applied electric field, reducing the effectively calculated mobility.[49,50] This can lead to time-dependent currents, electric field-dependent conductivities, and large hysteresis effects.[50,51] Many approaches have been reported to directly synthesize atomically precise metal NCs without further separation, which have been reviewed in detail.[52–54] For instance, size-focusing methodology has been used as a kinetically controlled protocol of the successful synthesis high-yield atomically precise Au NCs and become a universal method.[31,52,55,56] Novel ligand-exchange-induced size convention process originated from size-focusing method is able to achieve new magic sizes that cannot easily obtain by size-focusing.[57,58] Additionally, kinetically controlled size trapping method is another example for the synthesis of atomically precise NCs without any purification.[53] In other studies, few atom metal NCs byproducts attached to organic ligands can cause catalytic poisoning[59] and fluorescence quenching of the target Au NCs system.[60] It can be easy to separate the undesired byproducts when they are electrically charged, and the desired final products are uncharged. However, when the desired final products are also charged, for instance, in the case of $[Au_{25}(PPh_3)_{10}(PET)_5X_2]^{2+}$ where PET is 2-phenylethanethiol and X is Cl or Br,[50] the removal of byproducts is especially challenging. Similarly, for an NC-based device with improved performances and longevity, the NCs should also be highly stable under aerobic conditions. In the following section, we will highlight the general approaches taken in addressing the purity and stability issues for NCs.

2.1 | Purification approaches for NCs

Enormous efforts have been devoted to studying synthetic methods to obtain metal NCs in high quality.[9–12] Synthetic methods are in general categorized into two types, namely "top-down" and "bottom-up". The "top-down" approach includes chemically etching of larger metal NPs into the atomically precise desired final NCs products. For the etching processes, extra ligands such as phosphines (e.g., triphenylphosphine [TPP]) and thiols (e.g., PET) are often used.[31,61–63] Inevitably, some byproducts are generated during this etching process, often in much higher quantities than the desired final products[50] and must be filtered out of the solution to obtain relatively pure desired final products. On the other hand, in the "bottom-up" approach, metal NCs are synthesized by reducing metal ions in the presence of ligands.[21,64–66] One of the major problems in this approach is the formation of a mixture of different NCs (together with other impurities such as thiolates or even extras thiols) which needs further purification and isolation.[67] Great efforts have been consequently devoted to improving metal NCs uniformity with advanced techniques. Centrifugation or precipitation has been reported as a powerful separation tool.[50,68] For instance, Galchenko et al. achieved a highly pure Au_{25} NCs solution through repeated centrifugation steps in non-polar solvents prior to final precipitation in methanol or ethanol.[50] The synthesis of Au_{25} NCs through thiol etching from Au

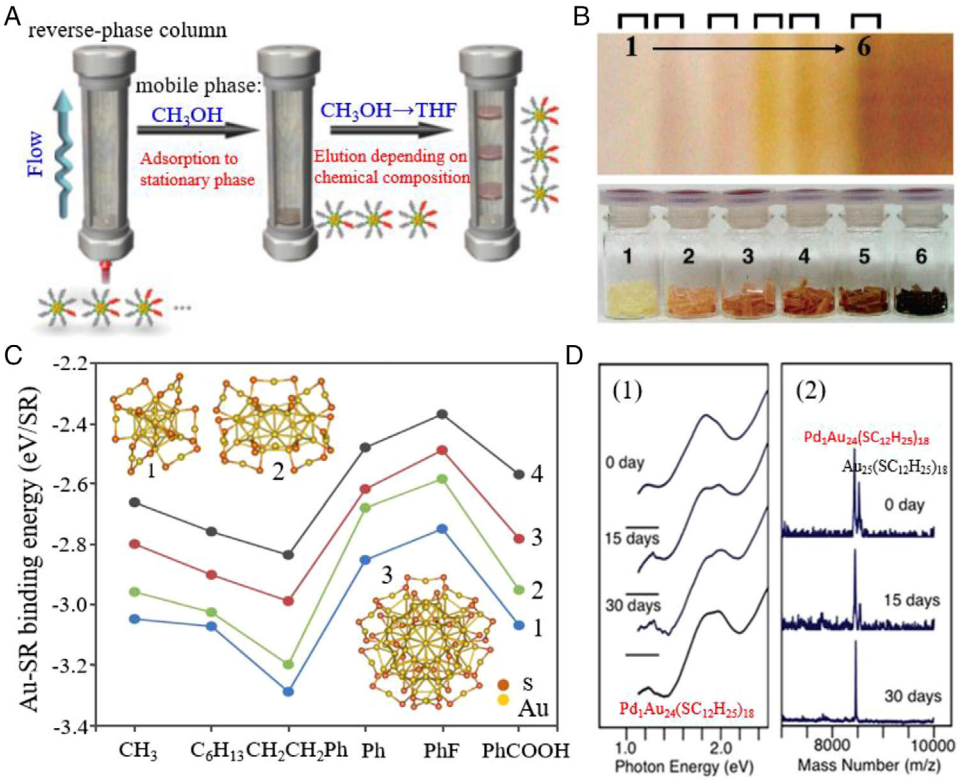

FIGURE 1 (A) Schematic view of the concept of a two-step separation of metal nanoclusters (NCs) mixture by high-performance liquid chromatography (HPLC). Reproduced with permission.[69] Copyright 2013, American Chemical Society. (B) The crude Au: SG NCs were separated into six components by a high-solution polyacrylamide gel electrophoresis (PAGE) (top). The appearance of gels containing fractionated NCs was shown individually (bottom). The numbers from 1 to 6 represent $Au_{18}(SG)_{11}$, $Au_{21}(SG)_{12}$, $Au_{25\pm1}(SG)_{14\pm1}$, $Au_{28}(SG)_{16}$, $Au_{32}(SG)_{18}$, and $Au_{39}(SG)_{23}$ NCs, respectively. Reproduced with permission.[75] Copyright 2004, American Chemical Society. (C) Reaction energies evaluated for the following reactions: $Au_{25}^- + 18SR \rightarrow Au_{25}(SR)_{18}^-$ (1), $Au_{38} + 24SR \rightarrow Au_{38}(SR)_{24}$ (2), and $Au_{102} + 44SR \rightarrow Au_{102}(SR)_{44}$ (3), compared with that of the simple case: $Au + SR \rightarrow AuSR$ (4). Insets are the illustration of crystal structures of $Au_{25}(SR)_{18}^-$, $Au_{38}(SR)_{24}$, and $Au_{102}(SR)_{44}$ NCs from 1 to 3. All the R moieties are omitted for clarity. Reproduced with permission.[85] Copyright 2012, The Royal Society of Chemistry. (D) Time-dependent stability investigation of $Au_{25}(SC_{12}H_{25})_{18}$ and $Pd_1Au_{24}(SC_{12}H_{25})_{18}$ NCs measured by absorption spectra (1), and MALDI-MS (2), respectively. Reproduced with permission.[92] Copyright 2010, The Royal Society of Chemistry

NPs precursor solution was tracked by UV-vis absorption spectroscopy. As the Au NPs were broken down into small-sized Au_{25} NCs, the intensity of the transition peaks between highest occupied molecular orbital and lowest unoccupied molecular orbital (HOMO-LUMO) increased. Mass spectrometry (MS) of the final products showed large quantities of $[Au_3TPP_3O_2]$ and $[Au_2TPP_2PET]^+$ byproducts, which were largely eliminated through the purification process described above. It was also shown that the initial concentration of the $[Au_3TPP_3O_2]$ byproducts could be significantly reduced by taking great care to reduce water residues and moisture in the initial synthesis reaction. Furthermore, the resulting highly pure Au_{25} NCs solution was used to form films by spin coating, and then their electrical transport properties were further investigated.[47] Many other similar strategies have been used for the purification of atomically precise NCs, since at this size range every atom matters.

Chromatographic approaches provide a new direction for the isolation of metal NCs. Niihori et al. reported a precise and systematic preparation of $PdAu_{24}(SC_{12}H_{25})_{18\text{-}n}(SBB)_n$ NCs (n = 6–16, SBB = 4-tert-butylbenzylmercaptan), which can be separated by using high-performance liquid chromatography (HPLC).[69] The separation is a two-step process (Figure 1A): Initially, the injection of the mixture of all NCs was adsorbed onto the stationary phase (the column matrix), followed by the elution of the adsorbed NCs from the column. The successful separation completed, thanks to the mobile phase gradually changed from pure methanol to tetrahydrofuran (THF) because the $PdAu_{24}(SC_{12}H_{25})_{18\text{-}n}(SBB)_n$ NCs are insoluble in methanol while dissolving in THF. The Murray group separated charged, non-uniformed, water-soluble Au NCs protected with monolayers of N-acetyl-L-cysteine and tiopronin ligands utilizing another ion-pair (ion-interaction) chromatography, which consists of necessary interaction between an ionic sample and a hydrophobic modifier counterion at a hydrophobic stationary-phase interface.[70] The same group described using reversed-phase (RP)-HPLC, with a C8 stationary phase column in series with a phenyl column, to separate the mixture of hexanethiolate-protected Au NCs of varying core sizes, elucidating a size exclusion-like separation mechanism.[71,72] The corresponding high-resolution separation of Au NCs with RP-HPLC has been reviewed in detail by Niihori et al.[73] An alternative, efficient thin-layer chromatography was also reported by Ghosh et al. to separate the mixture of Au NCs with different ligands and core sizes successfully.[74]

Polyacrylamide gel electrophoresis (PAGE) could isolate metal NCs protected with biological molecules based on their electrophoretic mobility in the past decades. Most of the previous reports using PAGE for NCs separation focus on glutathione (SG)-protected metal NCs.[21,67,75–77] For instance, Tsukuda's group presented that magic-numbered SG-protected Au_n NCs (n = 18, 21, 25, 28, 32, 39) can be sufficiently separated using high-resolution PAGE. The sample

was fractionated into six groups (Figure 1B).[75] These fractions from 1 to 6 are referred to as $Au_{18}(SG)_{11}$, $Au_{21}(SG)_{12}$, $Au_{25\pm1}(SG)_{14\pm1}$, $Au_{28}(SG)_{16}$, $Au_{32}(SG)_{18}$, and $Au_{39}(SG)_{23}$ NCs, respectively. In another work, the Pradeep group synthesized a crude mixture of red-fluorescent $Ag_8(H_2MSA)_8$ and bluish-green-fluorescent $Ag_7(H_2MSA)_7$ NCs by interfacial synthesis from $Ag@H_2MSA$ NPs precursor.[78] This Ag NCs mixture was separated into two bands (NCs) by PAGE: NC 1 was red under visible light excitation, while pink at 273 K under UV light excitation referred to as $Ag_8(H_2MSA)_8$ NCs and NC 2 referred to $Ag_7(H_2MSA)_7$ NCs was light yellow and bluish-green in visible and UV light illumination at room temperature, respectively.

An alternative method for NCs isolation is solvent extraction, which is based on the NCs' solubility in a different solvent. In the preparation of $Au_{38}(PhC_2S)_{24}$ NCs, the desired products were normally contaminated with large amounts of $Au_{140}(PhC_2S)_{53}$ NCs.[56] The pure $Au_{38}(PhC_2S)_{24}$ NCs can be obtained with the isolation from the mixture of $Au_{38}(PhC_2S)_{24}$ and $Au_{140}(PhC_2S)_{53}$ NCs treated with acetonitrile followed with filtering and evaporating, determined by ^1H NMR. The Tsukuda group also reported that the mixture of $[Au_{25}(SC_6H_{13})_{18}]^x$ (x = 1−, 0, and 1+)[79] and $Au:SC_n$ NCs (n = 6, 10, 12)[80] can be isolated using solvent extraction. Chen et al. prepared solvent-solvable $Au_{102}(SPh)_{44}$ NCs using acetone and CH_2Cl_2 to extract the small-sized Au NCs (<Au_{102}) and the desired products $Au_{102}(SPh)_{44}$ NCs, respectively, followed with size exclusion chromatography. The as-obtained pure $Au_{102}(SPh)_{44}$ NCs were confirmed by matrix-assisted laser desorption ionization (MALDI) and electrospray ionization MS, combined with UV-vis absorption spectroscopy and thermogravimetric analysis.

2.2 | Stability enhancement approaches for NCs

The unique physical and chemical properties of metal NCs make them widely applicable in various areas. The poor stability of some of these NCs, however, impedes them for further development especially in the case of device-based applications. Enormous effort has been devoted to enhancing the stability of NCs, and many methodologies were proposed. One of them is finding suitable ligands, contributing to the NCs' colloidal, electronic, thermal, and other stabilities.[81–84] Jung et al. investigated the electrochemical and thermodynamic stability of thiolate (SR)-protected Au NCs, $Au_m(SR)_n$, where R (aliphatic) = CH_3, C_6H_{13}, and CH_2CH_2Ph, and R (aromatic) = Ph, PhF and PhCOOH.[85] Three different NCs namely, $Au_{25}(SR)_{18}^-$, $Au_{38}(SR)_{24}$, and $Au_{102}(SR)_{44}$ were studied (Figure 1C, inset). By comparing the vertical ionization potential (VIP) and vertical electron affinity (VEA) of these NCs, a larger VIP-VEA value represented energetically nonconductive to activating the NCs to react, indicating high NCs electrochemical stability. They presented that the VIP-VEA values of aliphatic thiols are slightly higher than those of aromatic thiols in this work. Particularly, the VIP-VEA values for $-SCH_2CH_2Ph$ ligands are larger than those for -SPhCOOH ligand in three different NCs, suggesting the higher electrochemical stability of $-SCH_2CH_2Ph$ thiol. In addition, in terms of the thermodynamic stability against Au_m + nSR dissociation, the reaction energies were evaluated for the following reactions: Au_{25}^- + 18SR → $Au_{25}(SR)_{18}^-$, Au_{38} + 24SR → $Au_{38}(SR)_{24}$, and Au_{102} + 44SR → $Au_{102}(SR)_{44}$ compared with that of the simple case: Au + SR → AuSR. They concluded from Figure 1C that the NCs protected with aliphatic thiols (such as $-SCH_3$ ligands) have better electrochemical and thermodynamic stability than those with aromatic ones (such as -SPhCOOH ligands). Analogously, Zhang et al. studied the thermodynamic stabilities of anionic thiolated NCs $[M_{12}Ag_{32}(SR)_{30}]^{4-}$ with different ligands, where M = Ag, Au, and SR = SPhF, $SPhF_2$, and $SPhCF_3$.[86] It was found that NCs containing $SPhF_2$ are thermodynamically more stable than those with $SPhCF_3$ and SPhF. Negishi et al. proposed the Au_{25} NCs protected with octaneselenolate (SeR) to obtain $Au_{25}(SeR)_{18}$ NCs, which possess similar geometric structures to $Au_{25}(SR)_{18}$.[87] The charge transfer between the metal atoms and ligands of $Au_{25}(SeR)_{18}$ NCs was found to be lower than the latter. The results even pointed out that the metal-ligand binding in $Au_{25}(SeR)_{18}$ NCs was more covalent than those in $Au_{25}(SR)_{18}$ NCs. Later, the Negishi group synthesized Cu-doped Au NCs using SeR ligands to obtain $Cu_nAu_{25-n}(SeC_8H_{17})_{18}$ (n = 0–9). According to the data from MALDI-MS, the chemical composition of $Cu_nAu_{25-n}(SeC_8H_{17})_{18}$ was intact over this period in toluene at 25°C. By contrast, the analogous NCs with SR suffered from dissociation under the same conditions, which exhibit less stability.[88] Similarly, Zhu's group presented a ligand-exchange method to prepare $[Au_{25}(SePh)_{18}]^-[(C_8H_{17})_4N]^+$ NCs from the precursor $Au_{25}(SCH_2CH_2Ph)_{18}^-TOA^+$ NCs.[89] The UV-vis absorption spectra indicated that no manifest change was observed in these new $[Au_{25}(SePh)_{18}]^-$ NCs when dissolved in CH_2Cl_2 in air, which shows much better thermodynamic stability than their precursor. Hereafter, they also reported the transformation of Au NCs co-stabilized with SePh and 1,5-bis(diphenylphosphino)pentane (L^5 for short) to obtain $[Au_{11}(L^5)_4(SePh)_2]^+$ NCs.[90] The results showed that the optical absorption spectra of $[Au_{11}(L^5)_4(SePh)_2]^+$ NCs are nearly unchanged, exhibiting more thermodynamically stable than both $Au_{11}(PPh_3)_7Cl_3$ NCs and $Au_{11}(PPh_3)_8Cl_2$ NCs.

Alternatively, the strategy of foreign metal atom doping also exhibits a potential for improving the stability of metal NCs. To date, various metals including Pd, Pt, Cu, and Ag have been reported for metal-doped-NCs and showed the ability to alter the overall stability of metal NCs. Negishi et al. proposed a mono-Pd-doped $Au_{25}(SC_{12}H_{25})_{18}$ NC to fabricate $Pd_1Au_{25}(SC_{12}H_{25})_{18}$ NCs based on a previously reported synthesis protocol.[91] The results of time-dependent absorption spectra and MALDI-MS revealed that the $Pd_1Au_{24}(SC_{12}H_{25})_{18}$ NCs are more stable against degradation in solution (Figure 1D, (1)) and laser dissociation (Figure 1D, (2)), respectively, in comparison with $Au_{25}(SC_{12}H_{25})_{18}$ NCs with the same structure, indicating that the doping of a central atom is a powerful method to enhance the thermodynamic stability of metal NCs. Depending on the same principle, they further synthesized Ag-doped Au NCs to obtain $Au_{25-n}Ag_n(SR)_{18}$ (n = 0–11) using the same ligands.[92] In addition, the Jin group reported single-Pt-atom-doped $Au_{25}(SC_2H_4Ph)_{18}$ NCs.[93] They found that pure $Pt_1Au_{24}(SC_2H_4Ph)_{18}$ NCs can be obtained from the mixture of $Pt_1Au_{24}(SC_2H_4Ph)_{18}$ and

$Au_{25}(SC_2H_4Ph)_{18}$ NCs under treatment with concentrated hydrogen peroxide (H_2O_2). The results demonstrated that H_2O_2 can selectively decompose $Au_{25}(SC_2H_4Ph)_{18}$ NCs, indicating that $Pt_1Au_{24}(SC_2H_4Ph)_{18}$ NCs are more stable than $Au_{25}(SC_2H_4Ph)_{18}$ NCs. This greatly improved stability was ascribed to the stronger interaction between the central Pt and the Au_{12} icosahedral cage. Bootharaju et al. presented a compositionally uniform $[Ag_{24}Au(SR)_{18}]^-$ NC originated from a pure $[Ag_{25}(SR)_{18}]^-$ NC via a galvanic exchange protocol. It was shown that the successful exchange of the central Ag of Ag_{25} NCs with Au enhanced NC's stability significantly.[94]

Apart from the ligand-assisted and metal-doped methods, counter ions have also been validated by both, experimental and theoretical means, showing their probability to improve the NCs' stability. Yao and coworkers proposed an electrostatic interaction assisted stability enhancement approach for hydrophilic metal NCs coated with hydrophobic cations to about half of a monolayer coverage.[95] Zheng's group compared $[(PPh_3)_2N]^+$ and PPh_4^+ as counter cations to affect the thermodynamic stability of $[M_{12}Ag_{32}(SR)_{30}]^{4-}$ NCs, in which M represents Ag, Au, and SR represents SPhF, $SPhF_2$, and $SPhCF_3$.[86] They found that the $[(PPh_3)_2N]^+$ ions were deleterious to the NCs' stability. Moreover, the $(PPh_4)_4[Au_{12}Ag_{32}(SPhF_2)_{30}]$ NCs were reported to be more stable in dimethylformamide (DMF) than that in air, and that for more than 8 days.

3 | DEVICES WITH METAL NCs

Atomically precise metal NCs for various applications (i.e., imaging,[46,96–98] catalysts,[99–101] etc.) have been studied extensively, which derive from the unique physical characters of metal NCs and benefit from the rapid growth of the synthesis approaches for high-quality metal NCs. Opening up applicable devices with metal NCs in untapped research fields, similar to semiconductor areas, such as solar cells[1,102] and transistors[47,48], have attracted continuous attention in the nanomaterial research community in the last few years. Besides, fluorescent metal NCs provide convenience to fabricate colorimetric and fluorimetric sensing testers, which mostly depends on the fluorescence quenching of metal NCs.[103,104] We discuss above mentioned NC-based devices in detail by classifying them into different types of functions.

3.1 | MCSCs

SCs are the device of photovoltaic energy conversion.[105,106] Upon light irradiation, the photogenerated electrons and holes are generated as the light-induced transition from the ground state to the excited state. They are conveyed away by the electron or hole transport. The excited electrons must go through external applications involving an electrical load or some storage. For instance, a typical DSSC includes a nanocrystalline titanium dioxide (TiO_2) electrode coated with a dye on a transparent conducting oxide as the photoelectrode, an electrolyte solution based on dissolved iodide ion/triiodide ion (I^-/I_3^-) redox couple between the electrodes and platinum thin-film as the counter electrode. The primary charge-transfer process occurred at the TiO_2/dye/electrolyte interface. The light-induced transition of the sensitizer dye is from the ground state to the excited state, where the excited electrons were injected into the conduction band of TiO_2 and subsequent regeneration of the sensitizer dye by (I^-/I_3^-) redox couple.[41] Possessing molecule-like properties, metal NCs were found to be able to capture and converse incident photons to electricity.[102,107] Kamat group reported MCSCs using Au:SG NCs as sensitizers.[36] The as-prepared NCs exhibited orange emission with a maximum at 600 nm, indicating excited-state deactivation of these NCs through a radiative route. Typically, the working MCSC devices were fabricated by using the $Co(bpy)_3(PF_6)_2$/$Co(bpy)_3(PF_6)_3$ redox couple as the electrolyte, Pt-deposited fluorine-doped tin oxide (FTO) as the counter electrode, and the Au NCs-sensitized TiO_2 casted on FTO as the photoanode (Figure 2A). The mechanism of MCSCs was shown similarly to those found in both DSSCs and quantum dot-based solar cells (QDSCs). The external quantum efficiency or incident photon to photocurrent generation efficiency (IPCE) of MCSC was observed with its maximum IPCE of 70% at 400–425 nm, the region of which indicates the highly efficient conversion of captured incident photons to electrical energy. It was found that its highest IPCE was comparable to the CdS-based QDSC with IPCE value of 80%. In addition, the maximum PCE was 2.03–2.36% in MCSCs, close to 2–3% noted for CdS-based QDSCs. This high light conversion efficiency was ascribed to the higher HOMO-LUMO energy gap and stronger interaction with TiO_2, which enables effective electron injection. Additionally, the Co^{2+}/Co^{3+} redox couple, committing the delivery of steady photocurrent, contributed to the high PCE. Though such a great breakthrough with high efficiency has been achieved in MCSCs; however, a comprehensive understanding of which factors dictated light-harvesting efficiency in MCSCs is still limited. Abbas and coworkers, on the one hand, investigated the size effect of NCs on MCSC performance using four diverse-sized Au NCs, namely, $Au_{10\text{-}12}(SR)_{10\text{-}12}$, $Au_{15}(SR)_{13}$, $Au_{18}(SR)_{14}$, and Au_{25} $(SR)_{18}$ NCs (Figure 2B).[102] Among them, the highest PCE was observed in $Au_{18}(SR)_{14}$-based MCSCs with a value of 3.8%, superior to the previous report with 2.36 %,[36] which is attributed to their advantageous electron transfer kinetics and strong visible light-harvesting ability. On the other hand, the authors compared the open-circuit voltage (V_{OC}) and short-circuit current (J_{SC}) from current-voltage (J-V) curves of $Au_{18}(SR)_{14}$-based MCSCs with I^-/I^{3-} and Co^{2+}/Co^{3+} redox couples. The dramatic drop of J_{SC} in MCSC with the Co^{2+}/Co^{3+} redox couple resulted in a PCE decrease from 3.8% to 2.7%, since the bulky ligands of Co^{2+}/Co^{3+} would inhibit the effective mass transport. This indicated that this new record was in part because of the efficient redox couple I^-/I^{3-}. Recently, Stamplecoskie et al. proposed photovoltaics as a tool to determine the photocatalytic activities and some electronic properties of Au_x-SH NCs, and selected $Au_{18}(SR)_{14}$ NCs- and $Au_{25}(SR)_{18}$ NCs-MCSCs as models.[108] The result suggested that long-term stability and high solar energy harvesting efficiency were obtained in $Au_{18}(SR)_{14}/Co^{2+/3+}$ electrolyte-based MCSCs compared with those in I^-/I^{3-} electrolyte. Additionally, the HOMO energy of >0.95 eV was determined for this MCSC, which qualified it as promising candidate for photo-oxidation of substrates. Meanwhile, apart from the Au NC-MCSCs, other metal NC-based MCSCs have

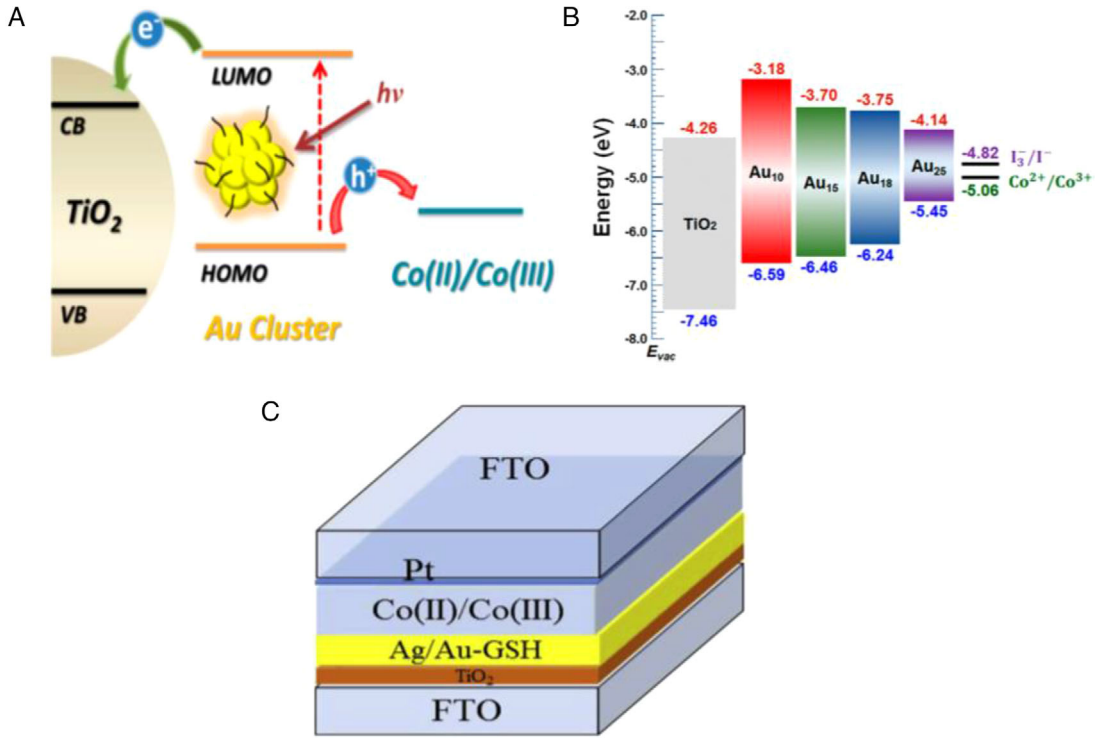

FIGURE 2 Representative demonstration of MCSCs: (A) Schematic illustration of the working principle of MCSCs. Reproduced with permission.[36] Copyright 2013, American Chemical Society. (B) Energy diagrams of TiO_2, Au NCs-sensitizers as well as redox couples. Reproduced with permission.[102] Copyright 2016, American Chemical Society. (C) Schematic structure of MCSC assembled with Ag-Au alloyed-sensitizers. Reproduced with permission.[117] Copyright 2015, Elsevier

also been reported. Bang's group proposed $Ag_{16}(SR)_9$-based MCSCs with I^-/I^{3-} electrolyte.[109] The V_{OC} and J_{SC} of the as-prepared MCSC were 650 mV and 617 $\mu A/cm^2$, respectively, which were five-fold superior to those found in previous reports, demonstrating the extensive potential of Ag NCs for further improvements of MCSCs. The PCE of Ag NCs-MCSCs was estimated to be 0.26%. It is found that, however, the intrinsic chemical and photochemical instability of Ag NCs under continuous illumination hinders the further application in MCSCs. Thus, the degradation mechanism of Ag NCs-modified photoelectrodes in MCSCs was further investigated.[110] The result indicated that the gradual transformation of Ag NCs to NPs under continuous illumination resulted in the decreased photocurrent. Hereafter, they devised a novel strategy to synthesize stable aggregation-induced emission (AIE) type Ag NCs with Ag(0)/Ag(I)-thiolate core/shell-structured NCs to tackle with the limitation of conventional Ag NCs as aforementioned.[111] It should be noted that AIE is an important mechanism for the strong luminescence emission of NCs, that is, non-luminescent oligomeric Au (I)-SR complexes are able to emit strong luminescence by aggregation and have been proved significantly important in various metal NC-based applications.[112–115] The presence of Ag(I)-thiolate complexes could significantly improve the stability of Ag NCs by preventing the Ag(0) core inside from being oxidized. As a result, an enhanced PCE of 1.40% was achieved, much higher than 0.26% of the conventional case,[109] offering an important milestone in the development of Ag NC-based MCSCs. Additionally, nanoalloy NC-MCSCs were first reported with Ag-Cu NCs by the Chen group.[116] Specifically, the authors utilized a spray-coating strategy to fabricate Ag-Cu bimetallic-NC-modified TiO_2 photoelectrodes. The syntheses of alloying NCs as Ag_1Cu_3, Ag_3Cu_1, and Ag_1Cu_1 were investigated in this study. The results indicated that MCSCs with a Cu-rich alloy exhibit the highest PCE (>1%) and possess more stable J_{SC} and V_{OC}, which are ascribed to the presence of Ag and Cu, respectively. Further mechanism investigations revealed that electron transfer in bimetallic Ag-Cu NCs occurs from Cu into Ag followed by the electron injection from Ag into the TiO_2 conduction band. In the monometallic case, the injection of electrons is simply from the NCs to the TiO_2 conduction band. In addition, they studied the influence of bimetallic Ag-Au NCs on the properties of MCSCs in comparison with monometallic Ag or Au NC-MCSCs (Figure 2C).[117] The photocurrent of alloyed Ag-Au NC-sensitized TiO_2 electrodes was constant, whereas those in both Ag-based and Au-based electrodes decreased, suggesting that alloyed NCs are beneficial to maintain the photocurrent stability of MCSCs. Besides, the bimetallic NC-MCSCs exhibited an enhanced J_{SC} and PCE compared to that of monometallic NC-MCSCs. These results illustrated that alloying NCs possess the potential to be a new class of photosensitizers. It should be noted, despite the fact that Pt and Pd NCs have been demonstrated to have photoelectrochemical properties, there are to the best of our knowledge not much reports on assembled MCSCs using these NCs.[118] Developing a suitable strategy for fabricating MCSCs using these metal NCs as photosensitizers is still challenging.

3.2 | Metal NC-based strain sensors

Flexible strain sensors can respond the mechanical deformations through changes in electrical signals (e.g., resistive- and capacitive-type sensors), monitoring the real-time human

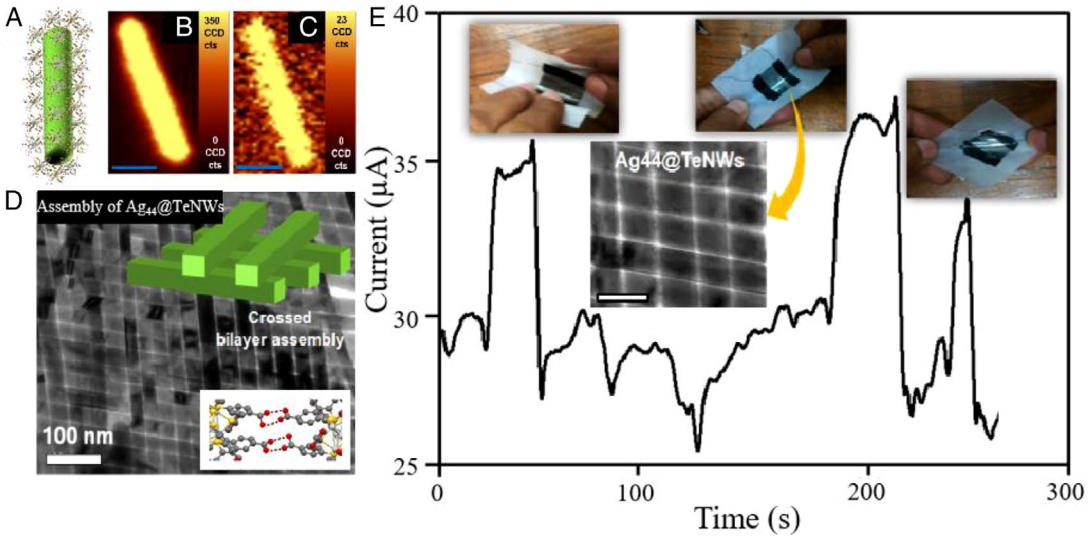

FIGURE 3 Representation of metal nanocluster (NC)-based strain sensors: (A) Schematic structural illustration of Ag_{44}@Te NWs. (B and C) Raman images showing the distribution of Te (B) and Ag_{44} NCs (C), respectively. (D) Transmission electron microscopy (TEM) image of the crossed assembly formed the bilayer structure of Ag_{44}@Te NW. The inset is a schematic of the assembly Ag_{44}@Te NW. (F) Conductivity change of the Ag_{44}@Te NW-based electronic device on polyethylene terephthalate substrate. Reproduced with permission.[122] Copyright 2016, Wiley-VCH

activities, have been successfully introduced, and recently received tremendous attention.[119–121] Basically, the strain sensor is composed of electrically conductive sensing films with flexible substrate for resistive-type sensor or a highly compliant dielectric layer between the stretchable electrodes pair for capacitive-type sensor, coupled with relatively simple read-out system. Thanks to ultra-small size and various functionalities, atomically precise NCs easily anchor on other nanostructures to constitute new composite structures, possessing new properties different from both, the NCs and the anchored units. Som et al. created bilayer assemblies of nanowires (NWs) by anchoring 44-silver-atom-NCs protected with para-mercaptobenzoic acid (p-MBA) as ligand, abbreviated as Ag_{44} (Figure 3A).[122] The Ag_{44} NCs were immobilized on the surface of Te NWs by mixing the precursor solutions in DMF. The structures were further purified by centrifugal precipitation of Ag_{44}@Te NWs. These composites exhibited features of both, Ag_{44} and Te NWs as confirmed from their optical spectra. Furthermore, a direct confirmation of Ag_{44} NCs anchored on the NWs was conducted by Raman spectroscopy. The corresponding intensity maps of the Te NWs (as measured by the characteristic Te Raman peak) and Ag_{44} NCs (as measured by the characteristic 4-MBA peak) are shown in Figure 3B,C, respectively. The assembly was created in an air-water interface similar to Langmuir–Blodgett film forming process. A transmission electron microscopy (TEM) image confirmed the crossed bilayer structure of the assembly, which happens at a specific NCs concentration on the surface of Te NWs (Figure 3D). This unusual bilayer structure was generated probably due to the formation of hydrogen-bonds of *p*-MBA ligands of two neighboring Ag_{44} NCs anchored to adjacent NWs. They further concluded that the greater number of hydrogen-bonding enhances the stability of Ag_{44}@Te NWs, which could be stable in air for weeks on suitable substrates. In addition, the potential application of this self-assembled thin film of Ag_{44}@Te NWs was conducted to be an electronic strain sensor (Figure 3E, inset). This device was fabricated by transferring Ag_{44}@Te NWs thin films on polyethylene terephthalate substrates. The electrical conductivity of the device altered when the substrate was bent, probably due to the change of the electrical resistance of the device (Figure 3E).

3.3 | Metal NC-based sensing devices

Many metal NCs have been designed to be a portable and simple device for rapid and sensitive detection of ions or small molecules. Among them, paper-based strip devices draw increasing attention. The basic sensing mechanism for the bio-/chemo-sensor was dependent on the rapid reaction between the analysts and sensor, characterized by colorimetric, fluorescent, and other methods.[103,123–126] Xie et al. proposed a facile non-labeled metal NC-based paper strip for the detection of Hg^{2+}.[123] This device was fabricated with bovine serum albumin (BSA)-modified Au NCs, which could be easily captured in the cellulose membrane with the conjugation of BSA. The detection based on the observation of the sample-induced color change under UV light (354 nm). The results showed that the strip fluoresces in weak green color (the background of cellulose membrane) in the presence of Hg^{2+} ions, while it exhibited red fluorescence upon the addition of other interference metal ions. The specific determination of Hg^{2+} with Au NCs was proven based on the metallic interaction of Hg^{2+} and Au^{+}, contributing to the quenching of fluorescence. Similarly, the Baker group designed a paper-based indicator strip with Au NCs@BSA incorporated within a sol-gel-derived mesoporous silica film for the fast and specific recognition of Hg^{2+} in aqueous streams. It even showed a pronounced quenching at the lowest concentration of 0.1 mM.[127] An alternative method for monitoring Hg^{2+} ions was developed based on electrospun membranes with BSA/poly(ethylene oxide) Au NCs (BSA/PEO-Au NCs).[124] The as-fabricated sensor showed good sensitivity toward Hg^{2+} ions with a limit of detection (LOD) as low as 57 pM. Later, Senthamizhan et al. presented a visually colorimetric detection of Hg^{2+} utilizing Au NCs integrated into polyvinyl alcohol (PVA) nanofibers, an elec-

trospun nanofibrous membrane (NFM), preparing composite AuNC*NFM, with an extremely low LOD of 1 ppb.[103] Alternatively, Ding and coworkers designed protein-Au NC-based paper test devices to probe Hg^{2+} ions.[128] The Au NCs were conjugated with enoyl-acyl carrier protein reductase (FabI), a drug target bacterial, producing Au NCs@FabI, which were entrapped onto nylon film by the electrostatic interaction between the positively charged nylon film and the negatively charged Au NCs@FabI at pH 7.4. By taking advantage of the specific interaction of Hg^{2+}-Au^{+}, the fluorescence signal can be quenched upon the addition of Hg^{2+}. BSA-capped Au NCs have been reported by Chanda's group to detect Pb^{2+} on paper substrates.[66] The quenching-based sensing mechanism was due to the metallophilic interaction of Au^{+} and Pb^{2+} similar to that of the detection of Hg^{2+} with Au NCs. The sensor showed an LOD of 1 ppb, which was 10-fold lower than the maximum level of drinking water set by the World Health Organization. Liu et al. proposed a user-friendly Ag NC-based paper strip for the detection of Cu^{2+}.[125] The Ag NCs synthesized with azobenzene modified poly(acrylic acid) (MPAA) were integrated onto the cellulose paper to fabricate the paper-based device. The fluorescence of Ag NCs was significantly quenched upon the addition of Cu^{2+}, which was attributed to the Cu^{2+}-Ag NCs binding and the energy transfer between them. In contrast, the fluorescence intensity was nearly unaltered in the presence of other interference metal ions and anions expect Ni^{2+} with a small extent of fluorescence quenched, showing its selective indication for Cu^{2+}. In another work, Senthamizhan et al. reported dithiothreitol (DTT) functionalized Au NCs (DTT.AuNCs) embedded in a porous cellulose acetate fiber for the determination of Cu^{2+}.[129] The further investigation of the sensing mechanism indicated that Cu^{2+} can be reduced to Cu^{+} by DTT and then react with Au through metallophilic interaction, thus resulting in effective fluorescence quenching. In another report, Ag NCs capped with polymethylacrylic acid were used in a paper-based strip for the colorimetric detection of Fe^{2+}.[130] The obvious color change on the strip can be easily observed by bare eyes due to the growth size of NCs to NPs induced by Fe^{2+}. In addition, this sensor exhibited good selectivity over other common anions due to the cation exchange property of the membrane.

In addition, great progress has been made concerning paper strip sensors with according Au NC-based multifunctional nanocomposites. Bothra et al. developed a BSA-Au NC based cellulose strip modified with vitamin B_6 cofactor pyridoxal for assaying Hg^{2+} up to 1 nM.[131] The practical application of this device was examined with water samples (tap water as well as river water), and samples from human beings (urine and plasma). More recently, Sun et al. proposed dual-emissive fluorescence detection of Hg^{2+} using two types of Au NCs, BSA-Au NCs and L-cysteine (Cys)-Au NCs. BSA-Au NCs emitting red color served as detecting probes, while Cys-Au NCs emitting blue color as reference.[126] The results indicated that the red fluorescence of the BSA-Au NCs was quenched upon the addition of Hg^{2+} in comparison with the intact blue fluorescence signal of Cys-Au NCs, enabling visually colorimetric detection of Hg^{2+} (Figure 4A). Wang's group presented a ratiometric test strip based on green emissive Au NCs doped in PVA films.[132] The Au NCs were first synthesized with glutathione (GSH) and mercaptopropionic acid (MPA), followed by the conjugation to the surface of silica NPs decorated with quantum dots (named as QD@SiO_2-MPTS). The green fluorescence of the Au NCs was quenched in the presence of Pb^{2+}, while the red fluorescence was still observed as internal reference. This device exhibited a visual LOD of 0.1 μM when indicating Pb^{2+} in water, showing its potential in on-site identification of Pb^{2+} without any elaborated equipment. Qi et al. reported the detection of Hg^{2+} with paper-based sensors embedded with Terbium(III)/gold NCs (Tb^{3+}/BSA-Au NCs) conjugates, where BSA-Au NCs work as signal probes while Tb^{3+} is used as a reference.[133] This Tb^{3+}/BSA-Au NCs-derived paper-based sensor can easily sense Hg^{2+} by using a handheld UV lamp. Upon the addition of Hg^{2+}, the visual fluorescence color change from red to green was evidenced under the illumination of a handheld UV lamp. Qiao et al. proposed fluorimetric paper strips based on Au-Ag NCs for probing Hg^{2+}.[104] The test strips were initially loaded with Au-Ag NCs followed with drying in the vacuum on the hydrophobic pattern, which could suppress "coffee stains" and warrant for the uniform distribution of the probes on the strips. Then the paper strips were treated with hydrophilic amine-derivatized silicane to obtain high aqueous stable and improved fluorescent probes. When exploring the probing selectivity of the fluorimetric paper strips, however, the interference of Cu^{2+} ions caused fluorescence quenching to some degree, which can be prevented with the introduction of ethylenediaminetetraacetic acid (EDTA), a strong chelating agent. The results indicated that higher sensitivity can be achieved with this developed fluorometric test strip, which exhibits good fluorescence quenching efficiencies (66%) in comparison with the commercial test strip (44%).

Additionally, the paper test sensors were achieved to determine multiple target analysts. The Sahoo group presented fluorescent turn-on easy probing of Zn^{2+} and Cd^{2+} with cellulosic strips with polyethyleneimine-modified Ag NCs (PEI-Ag NCs), which were conjugated with the B_6 cofactor pyridoxal 5′-phosphate (PLP), named as PLP_PEI-Ag NCs.[134] Irradiated under UV light at 365 nm, this PLP_PEI-Ag NCs modified paper strip exhibited yellow fluorescence, which can be changed to bluish-green when dipping in the solutions containing Zn^{2+} and Cd^{2+}, while no detectable fluorescence change was observed in the presence of other interference metal ions. Importantly, the yellow fluorescence can be recovered when the used bluish-green fluorescent strip is immersed in the solution of EDTA, showing its good reusability. Another interesting paper-based device using GSH-modified Au NCs fabricated by Bian et al. was used for the determination of Hg^{2+} and Pb^{2+}.[135] An obvious quenched and enhanced fluorescence was exhibited in the presence of Hg^{2+} and Pb^{2+}, respectively, contributing to the selective detection of these two ions over other metal ions. Similarly, the test strip showed good recyclability as the restoration of fluorescence could be achieved by dipping in the EDTA solution. A recent study reported by Sang et al. utilized methionine-modified Au NCs (Met-Au NCs) for the detection of Cu^{2+} and Co^{2+}.[136] The orange-red fluorescent test paper was quenched in the presence of Cu^{2+} and Co^{2+}, which can be easily recognized with the naked eye when illuminated with a UV lamp (365 nm excitation). Moreover, tartaric acid was selected to distinguish Cu^{2+} and Co^{2+}, in which the fluorescence quenched by Co^{2+} was restored while the quenched fluorescence by Cu^{2+} still remained unchanged even in the presence of tartaric acid.

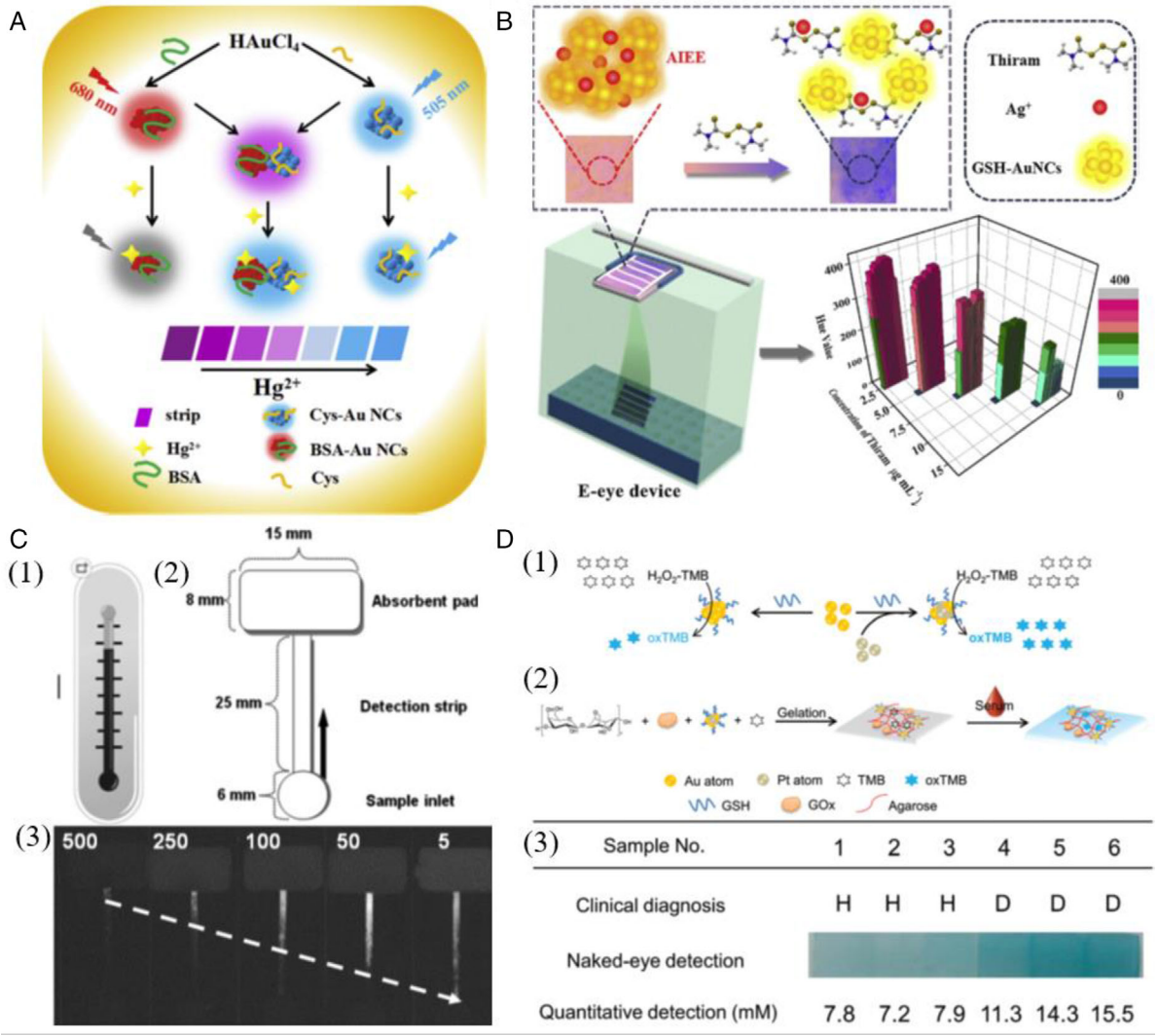

FIGURE 4 Representation of metal nanocluster (NC)-based devices on chemo-/bio-sensing: (A) Schematic illustration of the working principle of Cys/BSA-Au NCs fluorescent strips for sensitive determination of Hg^{2+}. Reproduced with permission.[126] Copyright 2019, Elsevier. (B) Schematic demonstration of the electronic-eye platform with Ag-Au NCs based on the AIEE effect for the detection of thiram. Reproduced with permission.[143] Copyright 2019, Elsevier. (C) Metal NC-based microfluidic sensor. (1) A thermometer-like BSA-Au NC-based platform for detecting Cu^{2+}. (2) Schematic demonstration of thermometer-like biosensor structure. (3) The pattern of fluorescence quenching in the presence of Cu^{2+}. The concentration of Cu^{2+} from left to right: 500, 250, 100, 50, and 5 μM, respectively. Reproduced with permission.[144] Copyright 2015, The Royal Society of Chemistry. (D) Au-Pt NC-based hydrogel film sensor. Schematic illustration of (1) sensing mechanism and (2) visual detection of glucose in human serum using Aga/Au–PtNCs/GOx/TMB hydrogel film sensor. (3) Practical investigation of this as-synthesized hydrogel film senor in human serum samples in comparison with clinical diagnosis results. "H" and "D" indicated those who were clinically diagnosed to be healthy and diabetic, respectively. Reproduced with permission.[99] Copyright 2017, The Royal Society of Chemistry

Additionally, NC-based paper strips have found their potential in determining some small molecules. Mathew et al. developed a BSA@Au NC-based sensor conjugated with the specific enzyme acetylcholinesterase (AChE) for the detection of acetylcholine (ACh).[137] AChE can cause the hydrolysis of ACh to choline, leading to the fluorescence quenching of the Au NCs. An on-off-on sensor presented by Zhao et al. for sensing GSH was fabricated based on Cu^{2+} functionalized transferrin coated Au NCs (Au NCs@Tf-Cu^{2+}).[138] Upon the introduction of Cu^{2+}, the fluorescence of the sensor was quenched and then recovered in the presence of GSH, while the sensor was inert to other biothiols such as Cys and homocysteine (Hcy), indicating this as-prepared sensor as a selectively sensing platform toward GSH. Interestingly, the Sony group proposed a paper-based probe with KI_3-quenched BSA-Au NCs to detect Cys and Hcy, which devoid the interference of GSH.[139] Upon the introduction of KI_3, due to the I_2 induced S-S bond forming between BSA, BSA-Au NCs aggregated, which can be confirmed by TEM images, and thus quenched fluorescence was observed thanks to energy transfer. When introducing the Cys/Hcy, which can reduce the S-S bond between BSA, the dissociation of NPs to Au NCs occurred, and the quenched fluorescence recovered. In addition, further studies indicated that Cys and Hcy can be distinguished through the pH value (6.0–10.6) because paper strips with Hcy maintained an obvious pink color up to a pH of 6.5 compared with the diminished color from the pH of 8.7 in the presence of Cys. Similarly, Wang et al. proposed a turn-on fluorescent paper strip for the determination of alkaline phosphatase (ALP) based on $KMnO_4$-quenched BSA-Au/Ag NCs, which were modified with ascorbic acid 2-phosphate (AAP).[140] Based on the catalysis mechanism, the AAP can be decomposed to ascorbic acid (AA) and phosphate catalyzed by ALP. As a result,

the as-produced AA in the absence of ALP can contribute to rescue the quenched fluorescence, leading to the restored fluorescence of Ag/Au NCs. Lu's group presented cytochrome c (Cyt c)-mediated GSH-Au NCs for monitoring trypsin.[141] The quenched and restored fluorescence was ascribed to the presence of Cyt c and trypsin, respectively. Significantly, the quantitative detection of trypsin can be achieved by combining a smartphone and the ImageJ software to be a promising platform for a point-of-care application. The Chen group developed BSA-Au NCs on a paper-based colorimetric platform for the determination of rifampicin, a common drug for inactive meningitis, cholestatic pruritus, and tuberculosis, in urine.[142] Upon the addition of rifampicin, the fluorescence of this as-prepared colorimetric assay got quenched, which can be easily observed with the aid of a digital camera.

In recent years, sensing pesticides utilized in agriculture became a research focus as they could give rise to the critical pollution of food and the environment. Yan et al. created chicken-egg-white-capped Au NCs for the sensitive assaying of paraoxon, a kind of organophosphorus pesticide.[37] This platform detected paraoxon in the medium of tyrosinase (TYR) and dopamine (DA). Initially, DA can be catalyzed to dopaminechrome by TYR, resulting in the effective fluorescence quenching of Au NCs. However, the introduction of paraoxon could impede the catalytic activity of TYR that contributed to the restoration of fluorescence intensity. Zhao et al. presented on-site detection of thiram with Ag^+-conjugated GSH-Au NCs probes based on the AIE enhancement (AIEE) effect.[143] Owing to the AIEE effect, the fluorescence of Au NCs was enhanced in the presence of Ag^+. However, upon the addition of thiram, the fluorescence-enhanced intensity was weakened due to the strong interaction between Ag^+ and thiram. Moreover, the paper strip was shown in an electronic-eye system with the aid of a smartphone, developing a user-friendly, portable, and simple platform for the detection of thiram (Figure 4B). Besides, the paper-based microfluidic sensor has emerged as another promising and rapid sensing strategy. For instance, Fang et al. developed a microfluidic sensor based on BSA-Au NCs for the determination of Cu^{2+}.[144] The fluorescence quenched when Cu^{2+} ions were flowing through the test strip (Figure 4C). In addition, it was reported that the LOD can be modulated by changing the water-absorbing capacity of the microfluidic sensor. An alternative detection for citrate was fabricated with Cys-Au NCs based on a paper-based microfluidic sensor.[145] The oxidation of 3,3′,5,5′-tetramethylbenzidine (TMB) can be induced by Cys-Au NCs upon the addition of H_2O_2 to generate a blue-colored product. However, the presence of citrate can be capped on the Au NCs' surface, which inhibited the catalytic activity of Cys-Au NCs, thus providing efficient colorimetric detection of citrate.

Apart from the paper-based device, metal NCs have been successfully utilized in other platforms such as hydrogel films, agar matrixes, glass slides, etc. for the target sensing. For example, Feng et al. presented a novel strategy for assaying glucose based on an agarose (Aga) hydrogel matrix, which consists of Au-Pt NCs, glucose oxidase (GOx), and TMB to form Aga/Au-Pt NCs/GOx/TMB sensor.[99] The TMB can be oxidized under NCs catalysts and generated a blue-colored product in the H_2O_2-mediated condition, in which the H_2O_2 was the by-product of the glucose oxidized by GOx (Figure 4D, (1)). For the practical investigation, glucose detection in human serum with this as-prepared platform was compared with clinical diagnosis (Figure 4D, (2, 3)). The highly consistent results indicated that it is a promising practical method to monitor glucose. Yin's group proposed Au NC-based membranes for assaying H_2O_2 with as-synthesized Au NCs casted in an agar matrix, which offers convenient transportation and long-term stability.[146] The research showed that this sensor was capable of visual detection of H_2O_2 in the range of 0–3.22 mM. Su et al. developed a glass-based sensor anchored with polyelectrolytes-conjugated BSA-Au NCs for the detection of Cu^{2+}.[147] The as-modified glass sensor exhibited fluorescence quenching toward both, Cu^{2+} and Hg^{2+}, while the presence of Sn^{2+} helped to distinguish Cu^{2+} from the interference of Hg^{2+}. Further studies showed that an excellent reusability of this sensor can be achieved using EDTA, which can be used for at least 15 times. Another interesting work toward Hg^{2+} sensing was proposed by the Pradeep group. They applied fluorescein isothiocyanate (FITC)-modified BSA-Au NCs as probes, which were embedded in Nylon-6 nanofibers based on a glass platform.[148] By taking advantage of the insensitivity of Hg^{2+} to the green fluorescent FTIC, the red fluorescence of Au NCs was quenched upon the introduction of Hg^{2+} ions, while the green fluorescence was evident under dark field fluorescence microscopy, demonstrating its selectivity to Hg^{2+} over other metal ions still with red fluorescence. Recent advances in chemo-/biosensors based on metal NCs are summarized in Table 1.

3.4 | Metal NC-based transistors

The field-effect transistor (FET) devices are composed of three terminals, source, gate, and drain corresponding to base, collector, and emitter of bipolar transistor, respectively, and possess the ability of controlling the conductivity between the drain and source varies by the electric gate field.[149,150] The electronic properties of metal NCs and NPs films are determined by the size of their metallic core, and the length and chemical composition of their colloid organic ligands, which give them colloidal stability in solution. A smaller core size will increase the energy gap between the discrete energy levels of the NCs and NPs, and longer organic ligands will increase the distance between the metallic cores, and thus decrease the coupling. Both characteristics will increase the resistance to electron transport in the film.

In NC and NP films at low temperature, charge transport is dominated by tunneling between the discrete energy levels of the individual metal nanocrystals.[151,152] This results in an electrostatic Coulomb repulsion between the charged metal NPs, which requires a minimum applied voltage to be overcome and for the charge to flow. In addition, a gate voltage can be used to charge the film and activate charge transport across the discrete energy barriers, leading to conductance spikes at certain gate voltages known as Coulomb oscillations. To observe such ordered Coulomb blockade behavior, well-ordered films of monodisperse MCs are necessary. The Langmuir–Blodgett (LB) method is one such way of preparing ordered monolayer films of metal NP, with great care necessity in optimizing the deposition parameters.[153] Highly ordered, LB-deposited CoPt NP monolayer films exhibit thermally activated hopping charge transport between

TABLE 1 Summary of recent advances in NCs-based chemo-/biosensors

Analyte	NC-based sensor	LOD/test range	Methods/mechanism	Device features	Reference
Metal ions					
Hg^{2+}	BSA-Au NCs	0.1 ppb	Fluorescence quenching of Au NCs by Hg^{2+}-Au^{+} interaction	Captured in the cellulose membrane	[123]
	AuNCs@BSA	0.1 mM	Fluorescence quenching of Au NCs by Hg^{2+}-Au^{+} interaction	Trapped in a sol-gel-derived mesoporous silica film	[127]
	BSA/PEO-Au NCs	57 pM	Fluorescence quenching of Au NCs by Hg^{2+}-Au^{+} interaction	Based on electrospun membranes	[124]
	AuNC*NFM	1 ppb	Visual fluorescent response to Hg^{2+}	Integrated into electrospun PVA nanofibers	[103]
	Au NCs@FabI	1 nM to 10 μM	Hg^{2+} ions quenched fluorescence signal from the membrane	Entrapped onto nylon film	[128]
	BSA-Au NC-B_6	up to 1 nM	Selective fluorescence quenching of Au NCs	Using cellulose strip	[131]
	BSA-Au NCs and Cys-Au NCs	9 nM	Hg^{2+}-induced red fluorescence quenching of the BSA-Au NCs while blue fluorescence signal of Cys-Au NCs is intact	Immobilized onto filter papers	[126]
	Tb^{3+}/BSA-Au NCs	1 nM	Ratiometric fluorescent probes based on the quenching signal of BSA-Au NCs and intact fluorescence of Tb^{3+} as a reference	Using filter papers	[133]
	Au-Ag NCs	0.1 mM	Fluorimetric analysis of Hg^{2+}	Porous test strip	[104]
	Au@BSA/FITC/N6	down to 1 ppt	Luminescence quenching of Au@BSA/FITC/N6 fibers due to Hg^{2+}	Embedded in Nylon-6 nanofibers based on a glass platform	[148]
Pb^{2+}	DTT-mediated AuNC@BSA	0–2.5 ppm	Fluoresence quenching by the metallophilic interaction of Au^{+} and Pb^{2+}	On paper substrates	[66]
	Au@GSH/MPA decorated with QD@SiO_2-MPTS	0.1 μM	Green fluorescence of the Au NCs was quenched in the presence of Pb^{2+}, while the observed red fluorescence as internal reference	PVA films	[132]
Cu^{2+}	Ag NCs-MPAA	20 μM	Fluorescence quenching of Ag NCs in the presence of Cu^{2+}	Integrated onto the cellulose paper	[125]
	DTT.AuNCs	50 ppb	Cu^{2+} can be reduced to Cu^{+} by DTT and then react with Au through metallophilic interaction	Embedded in a porous cellulose acetate fiber	[129]
	BSA-Au NCs	0.1-500 μM	Fluorescence quenching	Microfluidic sensor	[144]
	polyelectrolytes-conjugated BSA-Au NCs	100-500 μM	"Off-on" fluorescence signal by Cu^{2+} and EDTA	Glass-based sensor	[147]
Fe^{2+}	AgNCs-PMAA	50 μM	Due to the growth size of NCs to NPs induced by Fe^{2+} measured by the plasmonic band and by naked eye	Impregnated on a cellulose filter paper and then coated with an ion exchange polymeric membrane	[130]
Zn^{2+} and Cd^{2+}	PLP_PEI-Ag NCs		Fluorescence enhancement may be due to the tetragonal coordinative interaction of Zn^{2+}/Cd^{2+} with the imine-N and the hydroxyl (–OH) groups of PLP	Using cellulosic strips	[134]
Hg^{2+} and Pb^{2+}	GSH- Au NCs	5 μM (Hg^{2+}) and 50 μM (Pb^{2+})	Aggregation-inducedfluorescence quenching and aggregation-induced fluorescence enhancement of AuNCs by Hg^{2+} and Pb^{2+}, respectively	Using test papers	[135]
Cu^{2+} and Co^{2+}	Met-Au NCs	47 pM (Cu^{2+}) and 420 pM (Co^{2+})	Recognized with the naked eye when illuminated with a UV lamp (365 nm excitation)	Using filter papers	[136]
Molecules					
ACh	BSA@Au NC-AChE	10 nM	AchE can cause the hydrolysis of ACh to choline, leading to the fluorescence quenching of the Au NCs	Using filter papers	[137]

(Continues)

TABLE 1 (Continued)

Analyte	NC-based sensor	LOD/test range	Methods/mechanism	Device features	Reference
GSH	Au NCs@Tf-Cu^{2+}		Fluorescence of the sensor was quenched and then recovered in the presence of GSH	On treated filter paper strips	[138]
Cys and Hcy	KI_3-quenched BSA-Au NCs		When introducing the Cys/Hcy, which can reduce the S-S bond between BSA, the dissociation of NPs to Au NCs occurred and the quenched fluorescence recovered	On paper strips	[139]
ALP	$KMnO_4$-quenched BSA-Au/Ag NCs-AAP		AAP can be decomposed to AA and phosphate catalyzed by ALP. And generated AA in the absence of ALP can contribute to rescue the quenched fluorescence, leading to the restored fluorescence of Ag/Au NCs	On filter papers	[140]
Trypsin	Cyt c-mediated GSH-Au NCs	1-100 μg /ml	The quenched and restored fluorescence was ascribed to the presence of Cyt c and trypsin, respectively	On common absorbent paper	[141]
Rifampicin	BSA-Au NCs	5 μg/ml	Rifampicin, the fluorescence of this as-prepared colorimetric assay got quenched	On filter papers	[142]
Citrate	Cys-Au NCs	0.4 μM	Via the oxidation reaction of TMB by Cys-Au NCs in the presence of H_2O_2	A paper-based microfluidic sensor	[145]
Glucose	Aga/Au-Pt NCs/GOx/TMB sensor	0.34 mM	Au–PtNCs–GOx cascade-catalyzed system with H_2O_2 as the intermediate toward the oxidation of TMB	Based on an Aga hydrogel matrix	[99]
H_2O_2	Au NC-based membrance	0-3.22 mM	Luminescence quenching of Au NCs with H_2O_2	Loaded in an agar matrix	[146]
Pesticides					
Paraoxon	TYR-Au NCs- DA	5 ng /ml	Off-on fluorescence signal	On filter paper strips	[37]
Thiram	Ag^+-conjugated GSH-Au NCs	0.05 μg/ml	AIEE effect of strong interaction between Ag^+ and thiram	Paper strip with an electronic-eye system	[143]

Abbreviations: AA, ascorbic acid; AAP, ascorbic acid 2-phosphate; ACh, acetylcholine; AChE, acetylcholinesterase; AIEE, aggregation-induced emission enhancement; ALP, alkaline phosphatase; BSA, bovine serum albumin; DA, dopamine; DTT, dithiothreitol; EDTA, ethylenediaminetetraacetic acid; FITC, fluorescein isothiocyanate; GOx, glucose oxidase; GSH, glutathione; LOD, limit of detection; Met, methionine; NC, nanoclusters; NFM, nanofibrous membrane; PEI, polyethyleneimine; PEO, poly(ethylene oxide); PLP, pyridoxal 5′-phosphate; PVA, polyvinyl alcohol; TMB, tetramethylbenzidine; TYR, tyrosinase.

the metallic cores of the NPs at room temperature, with Coulomb blockade type transport between the discrete energy levels dominating at low temperature.[154] Transistor-like behavior can be observed for highly ordered monolayer films of highly monodisperse CoPt NPs at low temperature, where Coulomb blockade dominates charge transport. By applying a gate voltage in this regime, the films can be shifted from non-conducting to conducting states, as the energy levels between neighboring NPs are made to align, allowing charges to flow.[155] Depositing a monolayer film is critical to observe this Coulomb blockade behavior, since it allows all of the NPs to be affected simultaneously even by the applied gate voltage and prevents electrostatic screening between the NPs.[156] This has been achieved with 3.5 nm CoPt NPs and amine ligands, deposited onto electrical contacts via the Langmuir–Blodgett method. For temperatures below 90 K, the flat conductance observed around 0 V bias indicates that the charge transport in the film is dominated by Coulomb blockade. The Coulomb oscillations in these films were able to achieve on/off ratios of 90% at 10 K.[157]

Metal NCs, which are atomically precise, possess discrete energy levels while larger metal NPs have continuous bands.[158] These metal NCs are quite similar to semiconducting quantum dots because both exhibit discrete energy levels due to quantum confinement and are made colloidally stable by organic ligands surrounding their inorganic cores.[47,159,160] However, until recently, films of metal NCs had not shown semiconducting behavior yet, because the combination of core ligands had resulted in either Coulomb blockade behavior or band-like metallic transport.[161,162] The semiconducting behavior of NCs was first achieved in $[Au_{25}(PPh_3)_{10}(SC_2H_4Ph)_5X_2]^{2+}$ NCs, where X = Cl or Br (abbreviated as Au_{25}) by carefully tuning both the metal core and the surrounding organic ligands.[47] In this study, the FETs were fabricated by depositing Au_{25} films via spin coating. The transfer curves of an Au_{25} FET in Figure 5A clearly show an on/off ratio of 5×10^4 and a charge carrier mobility approaching 10^{-5} cm^2 V^{-1} s^{-1} at drain voltage (V_d) = 20 V, while the output curves indicate exponential behavior of the FET below a certain critical V_d (Figure 5B). Both types of curves reveal n-type transistor behavior of Au_{25} NCs in a film. The semiconducting properties of the film are further confirmed by their photoconductance, with increasing conductivity upon light illumination, as observed in the J-V curve in Figure 5C, (1). The transfer curve with and without illumination shows a shift in the doping of the transfer curve, which indicates that the dominant photoconduction mechanism is photogating (Figure 5C, (2)).

Very recently, Fetzer and co-workers presented an electrode device of single crystalline micro-crystals, which are

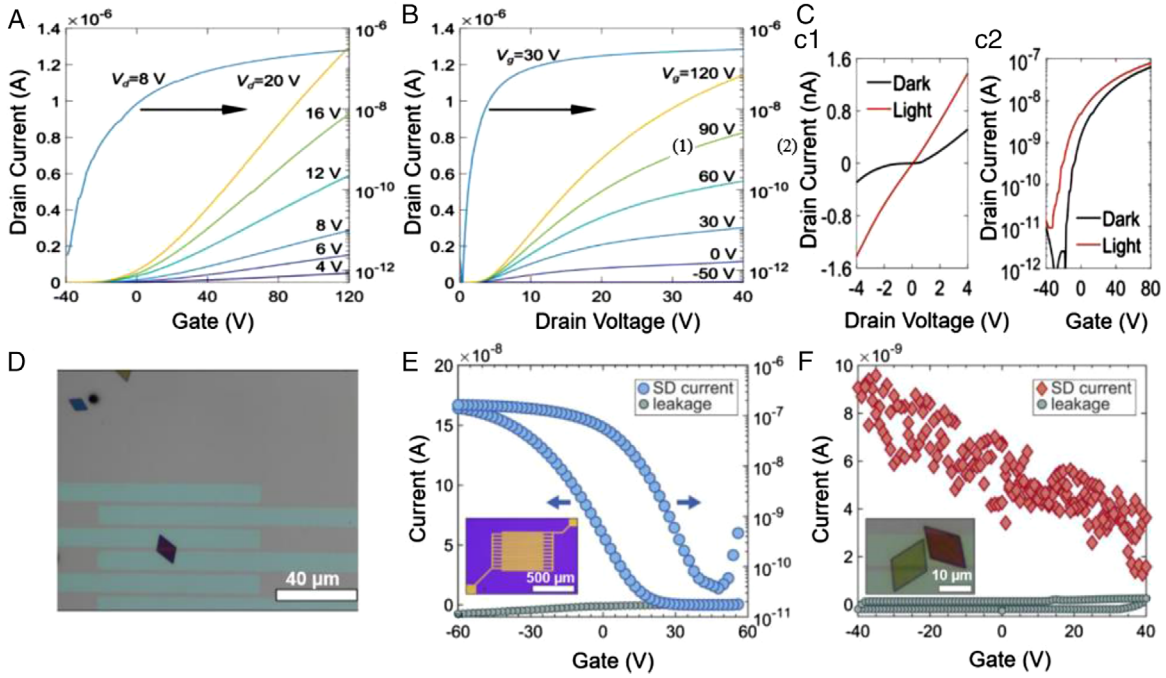

FIGURE 5 Representative electronic characterizations of nanocluster (NC)-based transistors: (A-C) Au_{25} NC films transistor: (A) Transfer and (B) output curves of field-effect transistor (FET), exhibiting clear transistor behavior. (C) Photoconductivity property: (1) J-V curves with V_g = 0 V and (2) transfer curves (V_d = 20 V) of Au_{25} NC films both in dark and irradiated with 635 nm laser. Reproduced with permission.[47] Copyright 2019, Wiley-VCH. (D-F) Au_{32}-NCs micro-crystal transistor: (D) Optical micrograph of Au electrode coated with micro-crystals on a Si/SiO_x device. (E and F) FET transfer curves of a polycrystalline film with Au_{32}-NCs device (E, blue dotted) and of an individual micro-crystal device (F, red dotted), respectively, in comparison with negligible leak current (grey dotted). Reproduced with permission.[48] Copyright 2020, ArXiv

self-assembled from $Au_{32}(^nBu_3P)_{12}Cl_8$ NCs (abbreviated as Au_{32}-NCs).[48] The Au_{32}-NCs in octane solution were dispersed onto an acetonitrile subphase, where they self-assembled into microcrystals as the acetonitrile solvent evaporated. The microcrystals then sank into a subphase, depositing onto the prefabricated electrodes, as shown in the optical image in Figure 5D. The electronic properties of micro-crystals and polycrystalline films were evaluated by FET measurements. The corresponding transfer curves are of a polycrystalline film of Au_{32}-NCs micro-crystals shown in Figure 5E, compared with the control experiment of an individual Au_{32}-NCs micro-crystal (Figure 5F). The results revealed that p-type behavior limited by Coulomb charging is observed in both cases, indicating holes as main charge carriers. The mean value of the hole mobility of single micro-crystal approaches 0.8×10^{-4} cm^2 V^{-1} s^{-1} at a source-drain voltage (V_{SD}) = 5 V (Figure 5F) which is a 100-fold decrease compared with that of micro-crystals deposited polycrystalline film (Figure 5E). These results were consistent with values found for previously reported FETs with Au_{25} NCs.[47]

Zheng's group reported a solvent-mediated assembly of intermetallic $(AuAg)_{34}$ NCs into one-dimensional polymeric $(AuAg)_{34n}$ with Ag-Au-Ag bonds between neighboring NCs.[163] The anisotropic structures of polymeric $(AuAg)_{34n}$ chains were confirmed by the parallel formation of $(AuAg)_{34n}$ NCs to the c-axis of the single crystal, which was separated in a- and b-axis by 1-ethynyladamantane ligands. FET devices were fabricated with monomeric $(AuAg)_{34}$ NCs and polymeric $(AuAg)_{34n}$ to detect the conductivity of the crystal. A single crystal of polymer NCs was transferred onto the Au electrode, in which the device channel was aligned with the a- or c-crystallographic axis. The average electrical conductivity along the c-crystallographic axis of the polymeric crystal showed near 1800-fold higher than those of the a-axis of polymeric $(AuAg)_{34n}$ NCs and of monomeric $(AuAg)_{34}$ NCs. This indicated that the -Ag-Au-Ag- chains in the polymeric crystal are advantageous to carrier transport. Further semiconductor measurements were conducted on single polymeric crystals along the c-axis. The transfer curves revealed p-type field effect, indicating a hole conduction mechanism, and showed an on/off current ratio of around 4×10^3, and the charge carrier mobility was calculated to be 2.46×10^{-2} cm^2 V^{-1} s^{-1} at V_{SD} = –16 V. It is worth noting that the mobility of the polymeric crystal is higher than for other reported NCs,[47,48] which is in the range of the common p-type single-crystal organic semiconductors[164] and close to that of CdSe QDs.[165]

3.5 | NC-based floating memory devices

Metal NP-based floating memory devices have been studied for over 10 years.[25,26] The floating memory device was developed consisting of a triple-layer structure of two semiconducting or insulating organic layers as well as a middle discontinuous metal layer, which were sandwiched between two metal electrodes.[25,166] The charge storage performances were evaluated using capacitance-voltage (C-V) and conductance−voltage (G−V) characterizations. Only recently, floating memory devices based on atomically precise Au NCs have been investigated. Hirata et al. fabricated NC-based floating memory devices consisting of uniform monolayer films of thiolated Au NCs (Au: SR, R = $C_{12}H_{25}$) formed by the Langmuir–Blodgett method, which are sandwiched between an insulating polymer film and a SiO_2 layer.

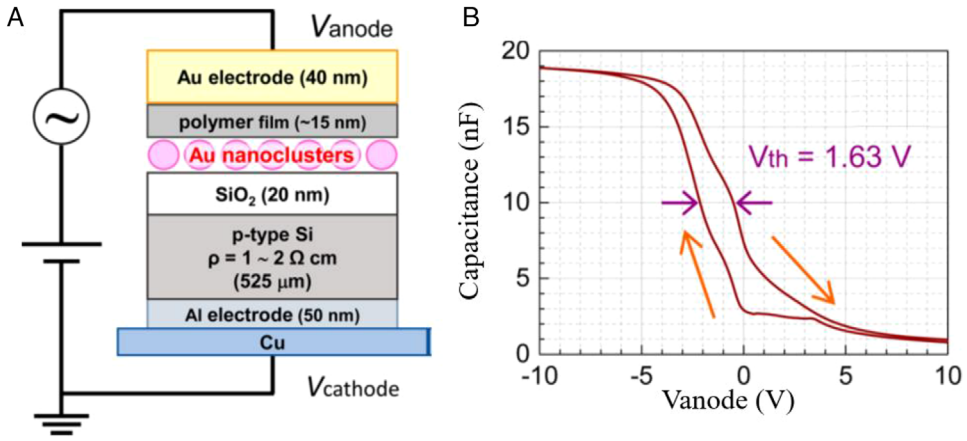

FIGURE 6 Representative illustration of nanocluster (NC)-based floating memory devices: (A) Schematic structure of an Au NC-based floating memory device. (B) The C-V curves with the largest V_{th} value of the floating memory device made using $Au_{38}(SR)_{24}$ NCs. Reproduced with permission.[167] Copyright 2017, American Chemical Society

(Figure 6A).[167] C-V measurements were used to evaluated electric properties of Au: SR-based floating memory devices. The negligible hysteresis was observed in the C-V measurements of the reference devices comprising a hydrophobic insulating layer with fluoropolymer (CYTOP) and without Au: SR NCs as an active layer. They found that the most effective devices, showing the largest voltage width (V_{th}) value of hysteresis curves, were made using $Au_{38}(SR)_{24}$ ($R = C_{12}H_{25}$), which possesses the largest energy gap between their HOMO and LUMO layers (Figure 6B). Further investigation on the frequency dependence of C-V and G−V was conducted in $Au_{38}(SR)_{24}$-based floating memory devices in comparison with the reference devices, confirming that the observed hysteresis originating from the Au: SR NCs. Further studies showed that similar behavior can be obtained for similar-sized Pd-doped Au (AuPd: SR) NCs in addition to Au: SR NCs.[168] Negative and positive shifts in C-V curves from reference measurements additionally showed that both, hole and electron injection from the Au electrodes to the NCs caused the observed hysteresis in the floating gate devices. The ratios of injected hole to injected electrons relied on the NCs' compositions and sizes, determined by the redox potentials of the NCs.

3.6 | NC-based other devices

Apart from the above mentioned NC-based device, very recently, Kim et al. proposed an exceptional solar-to-CO (STC) conversion with $Au_{25}(SR)_{18}$ (abbreviated as Au_{25}) electrolyzer immobilized on a gas diffusion electrode (GDE).[169] The system device was constructed with GDE-based Au_{25} powered by a $Ga_{0.5}In_{0.5}P/GaAs$ cell. The results showed that an STC conversion efficiency reached 18% over 12 h in 100% CO_2, whereas the efficiency of 15.9% was achieved in 10% CO_2 (typical CO_2 concentration of flue gas). Further kinetic investigations indicated that the high CO_2 reduction reaction (CO_2RR) performance was facilitated by the strong Au_{25}-CO_2 binding affinity. In addition, a high CO_2RR current density of 540 mA cm^{-2} was achieved in a gas-phase reactor.

More and more reports have been presented for the application of noble metal NCs as white light-emitting diodes (LEDs),[170–173] whereas Fu et al. proposed Cu NCs as the single phosphor for yellow and white LEDs with high efficiency, which probably due to the high photoluminescence quantum yield of Cu NCs synthesized.[174] Pradeep's group proposed atomically precise Ag NCs as one of the fluorophores for white light emitter, along with blue emission silicon NPs and green luminescent FITC.[175]

Kannan et al. devised an in situ impregnation method of Ag NCs in microporous chitosan-polyethylene glycol membranes for applications as drug delivery percutaneous device.[176] They found that the presence and increasing Ag NCs concentration hampered biofilm formation and stimulated cell viability and adhesion, enabling a sustainable release of an anti-inflammatory drug.

4 | FUTURE PERSPECTIVE

Metal NCs are a new class of alternatives to metal NPs and QDs in the field of nanoscience. The development in synthesis methods enables the derivation of well-defined size, shape, and morphology of NCs, resulting in various applications ranging from energy transfer devices to target sensors. These successes indicate that metal NCs possess a high potential for the application in multidisciplinary areas for advancing the development in both, fundamental and practical purposes. Despite fast-increasing strides that have been made with regard to the development of metal NC-based devices, many challenges still need to be settled in the near future. Therefore, we attempt to capture some of the existing aspects as follows.

4.1 | New synthetic approaches

Despite enormous attention having been focused on Au NCs with various synthesis protocols, other metal NCs (e.g. Pt, Pd, Ag, Cu), in part interesting alternatives to Au NCs, have gained little attention primarily due to their relative unstable chemical property as compared to Au NCs. In addition, the short excited-state lifetime of these alternatives NCs, to a great extent, hinders their further applications in terms of MCSCs. Moreover, the PCE of MCSCs

exhibited a relatively narrow visible light region compared to DSSCs or QDSCs, ascribing to the lack of absorbance in the entire visible or even near-infrared region. Taking the controlled-size and the choice of stabilized-ligands into consideration, the new-synthesized metal NCs would be expected to overcome these aforementioned conundrums. Besides, solvent-mediated assembly of metal NCs exhibited enhanced properties. Zheng's group synthesized $(AuAg)_{34n}$ NCs with anisotropic structure via a solvent-mediated assembly method.[163] The FET devices using these $(AuAg)_{34n}$ NCs succeeded in increasing the electrical conductivity and charge carrier mobility by several orders of magnitude, which indicates that the electron transport in assemblies of NCs is controlled by structural factors. This opens an opportunity to create structure-dependent metal NCs with desired structures and properties through the solvent-mediated synthesis approach.

4.2 | Complementary methodologies

Although many works have discussed bimetallic NC-based MCSCs in addition to monometallic NCs, the outcomes were not very satisfying. One possible approach is utilizing two or more sensitizers to settle this problem because the recently reported success in DSSCs using co-sensitization of zinc phthalocyanine and bithiophene-based organic dye to realize improved efficient light harvesting.[42,177] Besides, employing metal NC-based sensitizers with different spectral responses will, hopefully, result in a panchromatic MCSCs. Another approach to enhance the PCE of the MCSCs will be changing the adsorption mode of metal NCs on the TiO_2. Very recently, Abbas and coworkers proposed Au-NCs-based MCSCs with high PCE of 3.2% in the presence of Na^+ (alkali metal ions, AMI).[21] The hidden effect of AMI on metal NCs was suggested to change the adsorption strength between the NCs and TiO_2 with a chelating bonding, while ester-like bonding of NCs-TiO_2 interfaces in the absence of AMI. This research points out that the interfacial engineering strategy will improve NCs-based energy conversing device come true.

4.3 | Mechanism investigations

Recent advances unveil the atomically precise NCs with molecular- or atomic-level knowledge of formation and size evolution mechanisms.[178–181] These studies also promote the mechanism understanding of the metal NCs growth process and their intrinsic physiochemistry properties. Still, inherent challenges of similar molecular- or atomic-level mechanism advances of the metal NCs will remain a fundamental focus in the application research of metal NCs for further advancement.

4.4 | Stability characterizations

An important parameter of the applicable metal NC-based device is the stability of metal NCs. Enormous studies have proved that the fascinating properties of NCs are strongly dependent on the stability, and further enhancement in stability was shown ubiquitous.[87,93,94] Most of the literature discussed the stability of metal NCs before incorporating them into a device. However, such investigations were not continuous to the application as device, like "How the size and composition changes in device before and after being tested?" Such studies are expected to indicate the stability in NC science, which is vital to understanding the why and how these stable metal NCs influence the device properties.

4.5 | Alternatives to semiconductor-based devices

The electronic and optical properties of metal NCs are analogous to that of semiconductors. Recent progress regarding solar cells, memory devices, transistors, and sensors utilizing metal NCs as alternatives to semiconductors have been investigated successfully. This suggests a new direction in that metal NCs can be used in other semiconductor-like devices. The challenges of these devices with semiconductor-based thin films is stemming from the low long-range order, grain boundaries, and defects,[182] thus finding suitable substitute candidates is needed. To this end, metal NCs can function as promising materials in these applications. We hope that, in the near future, these metal NCs, possessing interesting electronic, optical properties, can find their places in the areas of power devices, next-generation multivalued or flash memory devices, integrated optical modulators, on-chip optical communications, and other optoelectronic devices. Hopefully, metal NCs, like semiconductors, can be implemented in some indispensable applications for daily life, such as displays, computers, telephones, and so forth.

Overall, metal NCs have been immensely explored in terms of devices owing to their intrinsically extraordinary properties. With regard to new phenomena of metal NCs, further experiments and theoretical studies are needed to understand the fundamental mechanism in detail. We hope that this review will provide a useful source of references for readers in the field of nanomaterials and promote applications with these nanomaterials.

ACKNOWLEDGMENTS

Lizhen Chen acknowledges the financial support offered by the Chinese Scholarship Council (CSC) for a PhD fellowship. Indranath Chakraborty thanks Fonds der Chemischen Industrie im Verband der Chemischen Industrie for the support. This work is supported by the Cluster of Excellence "Advanced Imaging of Matter" of the Deutsche Forschungsgemeinschaft (DFG) - EXC 2056 - project ID 390715994.

CONFLICT OF INTEREST

The authors declare no conflict of interest.

ORCID

Indranath Chakraborty https://orcid.org/0000-0003-4195-9384

REFERENCES

1. H. Choi, W. T. Chen, P. V. Kamat, *ACS Nano* **2012**, *6*, 4418.
2. N. Elahi, M. Kamali, M. H. Baghersad, *Talanta* **2018**, *184*, 537.
3. Z. Zhang, H. Wang, Z. Chen, X. Wang, J. Choo, L. Chen, *Biosens. Bioelectron.* **2018**, *114*, 52.

4. P. Yang, J. Zheng, Y. Xu, Q. Zhang, L. Jiang, *Adv. Mater.* **2016**, *28*, 10508.
5. X. Fu, J. Cai, X. Zhang, W.-D. Li, H. Ge, Y. Hu, *Adv. Drug Deliv. Rev.* **2018**, *132*, 169.
6. I. Fratoddi, I. Venditti, C. Battocchio, L. Carlini, S. Amatori, M. Porchia, F. Tisato, F. Bondino, E. Magnano, M. Pellei, C. Santini, *Nanomaterials* **2019**, *9*, 772.
7. K. Kluczyk, L. Jacak, W. Jacak, C. David, *Materials* **2018**, *11*, 1077.
8. L. Liu, A. Corma, *Chem. Rev.* **2018**, *118*, 4981.
9. S. Guo, E. Wang, *Nano Today* **2011**, *6*, 240.
10. H. Choi, S.-J. Ko, Y. Choi, P. Joo, T. Kim, B. R. Lee, J.-W. Jung, H. J. Choi, M. Cha, J.-R. Jeong, I.-W. Hwang, M. H. Song, B.-S. Kim, J. Y. Kim, *Nat. Photonics* **2013**, *7*, 732.
11. T. Kim, S. Kang, J. Heo, S. Cho, J. W. Kim, A. Choe, B. Walker, R. Shanker, H. Ko, J. Y. Kim, *Adv. Mater.* **2018**, *30*, 1800659.
12. I. Matsui, *J. Chem. Eng. Jpn.* **2005**, *38*, 535.
13. J. J. Yoo, G. Seo, M. R. Chua, T. G. Park, Y. Lu, F. Rotermund, Y.-K. Kim, C. S. Moon, N. J. Jeon, J.-P. Correa-Baena, V. Bulović, S. S. Shin, M. G. Bawendi, J. Seo, *Nature* **2021**, *590*, 587.
14. M. Saliba, W. Zhang, V. M. Burlakov, S. D. Stranks, Y. Sun, J. M. Ball, M. B. Johnston, A. Goriely, U. Wiesner, H. J. Snaith, *Adv. Funct. Mater.* **2015**, *25*, 5038.
15. J. Y. Kim, J.-W. Lee, H. S. Jung, H. Shin, N.-G. Park, *Chem. Rev.* **2020**, *120*, 7867.
16. P. V. Kamat, *J. Phys. Chem. Lett.* **2013**, *4*, 908.
17. Y. H. Jang, Y. J. Jang, S. Kim, L. N. Quan, K. Chung, D. H. Kim, *Chem. Rev.* **2016**, *116*, 14982.
18. Z. Hu, J. Wang, X. Ma, J. Gao, C. Xu, K. Yang, Z. Wang, J. Zhang, F. Zhang, *Nano Energy* **2020**, *78*, 105376.
19. M. A. Green, S. Pillai, *Nat. Photonics* **2012**, *6*, 130.
20. J. A. Anta, E. Guillén, R. Tena-Zaera, *J. Phys. Chem. C* **2012**, *116*, 11413.
21. M. A. Abbas, R. Thota, K. Pyo, D. Lee, J. H. Bang, *ACS Energy Lett*. **2020**, 1404.
22. J. Gopinath, R. K. C. Balasubramanyam, V. Santosh, S. K. Swami, D. K. Kumar, S. K. Gupta, V. Dutta, K. R. Reddy, V. Sadhu, A. V. S. Sainath, *Chem. Eng. J.* **2019**, *358*, 1166.
23. S. Pillai, M. A. Green, *Sol. Energy Mater. Sol. Cells* **2010**, *94*, 1481.
24. P. F. Lee, J. Y. Dai, *Nanotechnology* **2010**, *21*, 295706.
25. W. L. Leong, P. S. Lee, S. G. Mhaisalkar, T. P. Chen, A. Dodabalapur, *Appl. Phys. Lett.* **2007**, *90*, 042906.
26. J.-Y. Tseng, C.-W. Cheng, S.-Y. Wang, T.-B. Wu, K.-Y. Hsieh, R. Liu, *Appl. Phys. Lett.* **2004**, *85*, 2595.
27. Y. Tao, M. Li, J. Ren, X. Qu, *Chem. Soc. Rev.* **2015**, *44*, 8636.
28. I. Chakraborty, T. Pradeep, *Chem. Rev.* **2017**, *117*, 8208.
29. M. Gharib, M. Galchenko, C. Klinke, W. J. Parak, I. Chakraborty, *Nano Select* **2021**, *2*, 831.
30. R. Jin, *Nanoscale* **2015**, *7*, 1549.
31. M. Zhu, E. Lanni, N. Garg, M. E. Bier, R. Jin, *J. Am. Chem. Soc.* **2008**, *130*, 1138.
32. Y. Zeng, S. Havenridge, M. Gharib, A. Baksi, K. L. D. M. Weerawardene, A. R. Ziefuß, C. Strelow, C. Rehbock, A. Mews, S. Barcikowski, M. M. Kappes, W. J. Parak, C. M. Aikens, I. Chakraborty, *J. Am. Chem. Soc.* **2021**, *143*, 9405.
33. S. Maity, D. Bain, A. Patra, *Nanoscale* **2019**, *11*, 22685.
34. C. M. Aikens, *Acc. Chem. Res.* **2018**, *51*, 3065.
35. Y. Li, M. Zhou, R. Jin, *Adv. Mater.* **2021**, *294*, 2006591.
36. Y.-S. Chen, H. Choi, P. V. Kamat, *J. Am. Chem. Soc.* **2013**, *135*, 8822.
37. X. Yan, H. Li, T. Hu, X. Su, *Biosens. Bioelectron.* **2017**, *91*, 232.
38. B. Liu, H. Yao, W. Song, L. Jin, I. M. Mosa, J. F. Rusling, S. L. Suib, J. He, *J. Am. Chem. Soc.* **2016**, *138*, 4718.
39. L. Chen, S. Azeem, M. Ruan, W. Xu, A. Barck, A. Kornowski, W. J. Parak, I. Chakraborty, *Nano Select* **2021**, *2*, 758.
40. L. Zhu, Y. Zeng, M. Teubner, B. Grimm-Lebsanft, A. R. Ziefuß, C. Rehbock, M. A. Rübhausen, S. Barcikowski, W. J. Parak, I. Chakraborty, *ACS Appl. Nano. Mater.* **2021**, *4*, 3197.
41. E. Palomares, J. N. Clifford, S. A. Haque, T. Lutz, J. R. Durrant, *Chem. Commun.* **2002**, 1464. https://doi.org/10.1039/B202515A
42. L. Yu, K. Fan, T. Duan, X. Chen, R. Li, T. Peng, *ACS Sustain. Chem. Eng.* **2014**, *2*, 718.
43. D. K. Roh, W. S. Chi, H. Jeon, S. J. Kim, J. H. Kim, *Adv. Funct. Mater.* **2014**, *24*, 379.
44. D. C. Lim, B. Y. Seo, S. Nho, D. H. Kim, E. M. Hong, J. Y. Lee, S.-Y. Park, C.-L. Lee, Y. D. Kim, S. Cho, *Adv. Energy Mater.* **2015**, *5*, 1500393.
45. T. Klar, M. Perner, S. Grosse, G. v. Plessen, W. Spirkl, J. Feldmann, *Phys. Rev. Lett.* **1998**, *80*, 4249.
46. L. Zhang, E. Wang, *Nano Today* **2014**, *9*, 132.
47. M. Galchenko, A. Black, L. Heymann, C. Klinke, *Adv. Mater.* **2019**, *31*, 1900684.
48. F. Fetzer, A. Maier, M. Hodas, O. Geladari, K. Braun, A. J. Meixner, F. Schreiber, A. Schnepf, M. Scheele, *arXiv* **2020**, *2002*, 06454.
49. H. Nakanishi, D. A. Walker, K. J. M. Bishop, P. J. Wesson, Y. Yan, S. Soh, S. Swaminathan, B. A. Grzybowski, *Nat. Nanotechnol.* **2011**, *6*, 740.
50. M. Galchenko, R. Schuster, A. Black, M. Riedner, C. Klinke, *Nanoscale* **2019**, *11*, 1988.
51. D. Li, H. Wu, H.-C. Cheng, G. Wang, Y. Huang, X. Duan, *ACS Nano* **2016**, *10*, 6933.
52. R. Jin, C. Zeng, M. Zhou, Y. Chen, *Chem. Rev.* **2016**, *116*, 10346.
53. Q. Yao, T. Chen, X. Yuan, J. Xie, *Acc. Chem. Res.* **2018**, *51*, 1338.
54. Q. Yao, X. Yuan, T. Chen, D. T. Leong, J. Xie, *Adv. Mater.* **2018**, *30*, 1802751.
55. M. W. Heaven, A. Dass, P. S. White, K. M. Holt, R. W. Murray, *J. Am. Chem. Soc.* **2008**, *130*, 3754.
56. R. L. Donkers, D. Lee, R. W. Murray, *Langmuir* **2004**, *20*, 1945.
57. C. Zeng, H. Qian, T. Li, G. Li, N. L. Rosi, B. Yoon, R. N. Barnett, R. L. Whetten, U. Landman, R. Jin, *Angew. Chem. Int. Ed.* **2012**, *51*, 13114.
58. C. Zeng, Y. Chen, A. Das, R. Jin, *J. Phys. Chem. Lett.* **2015**, *6*, 2976.
59. T. A. Dreier, O. Andrea Wong, C. J. Ackerson, *Chem. Commun.* **2015**, *51*, 1240.
60. C.-A. J. Lin, T.-Y. Yang, C.-H. Lee, S. H. Huang, R. A. Sperling, M. Zanella, J. K. Li, J.-L. Shen, H.-H. Wang, H.-I. Yeh, W. J. Parak, W. H. Chang, *ACS Nano* **2009**, *3*, 395.
61. H. Qian, Y. Zhu, R. Jin, *ACS nano* **2009**, *3*, 3795.
62. L. C. McKenzie, T. O. Zaikova, J. E. Hutchison, *J. Am. Chem. Soc.* **2014**, *136*, 13426.
63. R. Jin, C. Liu, S. Zhao, A. Das, H. Xing, C. Gayathri, Y. Xing, N. L. Rosi, R. R. Gil, R. Jin, *ACS Nano* **2015**, *9*, 8530.
64. J. Xie, Y. Zheng, J. Y. Ying, *J. Am. Chem. Soc.* **2009**, *131*, 888.
65. K.-T. Chuang, Y.-W. Lin, *J. Phys. Chem. C* **2017**, *121*, 26997.
66. P. Nath, M. Chatterjee, N. Chanda, *ACS Appl. Nano Mater*. **2018**, *1*, 5108.
67. Y. Negishi, K. Nobusada, T. Tsukuda, *J. Am. Chem. Soc.* **2005**, *127*, 5261.
68. R. L. Whetten, J. T. Khoury, M. M. Alvarez, S. Murthy, I. Vezmar, Z. L. Wang, P. W. Stephens, C. L. Cleveland, W. D. Luedtke, U. Landman, *Adv. Mater.* **1996**, *8*, 428.
69. Y. Niihori, M. Matsuzaki, T. Pradeep, Y. Negishi, *J. Am. Chem. Soc.* **2013**, *135*, 4946.
70. M. M. F. Choi, A. D. Douglas, R. W. Murray, *Anal. Chem.* **2006**, *78*, 2779.
71. V. L. Jimenez, M. C. Leopold, C. Mazzitelli, J. W. Jorgenson, R. W. Murray, *Anal. Chem.* **2003**, *75*, 199.
72. R. L. Wolfe, R. W. Murray, *Anal. Chem.* **2006**, *78*, 1167.
73. Y. Niihori, C. Uchida, W. Kurashige, Y. Negishi, *Phys. Chem. Chem. Phys.* **2016**, *18*, 4251.
74. A. Ghosh, J. Hassinen, P. Pulkkinen, H. Tenhu, R. H. A. Ras, T. Pradeep, *Anal. Chem.* **2014**, *86*, 12185.
75. Y. Negishi, Y. Takasugi, S. Sato, H. Yao, K. Kimura, T. Tsukuda, *J. Am. Chem. Soc.* **2004**, *126*, 6518.
76. I. Russier-Antoine, F. Bertorelle, M. Vojkovic, D. Rayane, E. Salmon, C. Jonin, P. Dugourd, R. Antoine, P.-F. Brevet, *Nanoscale* **2014**, *6*, 13572.
77. F. Bertorelle, R. Hamouda, D. Rayane, M. Broyer, R. Antoine, P. Dugourd, L. Gell, A. Kulesza, R. Mitrić, V. Bonačić-Koutecký, *Nanoscale* **2013**, *5*, 5637.
78. T. Udaya Bhaskara Rao, T. Pradeep, *Angew. Chem. Int. Ed.* **2010**, *49*, 3925.
79. Y. Negishi, N. K. Chaki, Y. Shichibu, R. L. Whetten, T. Tsukuda, *J. Am. Chem. Soc.* **2007**, *129*, 11322.
80. N. K. Chaki, Y. Negishi, H. Tsunoyama, Y. Shichibu, T. Tsukuda, *J. Am. Chem. Soc.* **2008**, *130*, 8608.
81. M. G. Taylor, G. Mpourmpakis, *Nat. Commun.* **2017**, *8*, 15988.
82. Q. Tang, R. Ouyang, Z. Tian, D.-E. Jiang, *Nanoscale* **2015**, *7*, 2225.
83. Y. Li, R. Juarez-Mosqueda, Y. Song, Y. Zhang, J. Chai, G. Mpourmpakis, R. Jin, *Nanoscale* **2020**, *12*, 9423.

84. X. Yuan, N. Goswami, I. Mathews, Y. Yu, J. Xie, *Nano Res* **2015**, *8*, 3488.
85. J. Jung, S. Kang, Y.-K. Han, *Nanoscale* **2012**, *4*, 4206.
86. X. Zhang, H.-Y. Yang, X.-J. Zhao, Y. Wang, N.-F. Zheng, *Chin. Chem. Lett.* **2014**, *25*, 839.
87. Y. Negishi, W. Kurashige, U. Kamimura, *Langmuir* **2011**, *27*, 12289.
88. W. Kurashige, K. Munakata, K. Nobusada, Y. Negishi, *Chem. Commun.* **2013**, *49*, 5447.
89. X. Meng, Q. Xu, S. Wang, M. Zhu, *Nanoscale* **2012**, *4*, 4161.
90. X. Kang, Y. Song, H. Deng, J. Zhang, B. Liu, C. Pan, M. Zhu, *RSC Adv.* **2015**, *5*, 66879.
91. Y. Negishi, W. Kurashige, Y. Niihori, T. Iwasa, K. Nobusada, *Phys. Chem. Chem. Phys.* **2010**, *12*, 6219.
92. Y. Negishi, T. Iwai, M. Ide, *Chem. Commun.* **2010**, *46*, 4713.
93. H. Qian, D.-E. Jiang, G. Li, C. Gayathri, A. Das, R. R. Gil, R. Jin, *J. Am. Chem. Soc.* **2012**, *134*, 16159.
94. M. S. Bootharaju, C. P. Joshi, M. R. Parida, O. F. Mohammed, O. M. Bakr, *Angew. Chem. Int. Ed.* **2016**, *55*, 922.
95. Q. Yao, X. Yuan, Y. Yu, Y. Yu, J. Xie, J. Y. Lee, *J. Am. Chem. Soc.* **2015**, *137*, 2128.
96. Y. Zhang, C. Zhang, C. Xu, X. Wang, C. Liu, G. I. N. Waterhouse, Y. Wang, H. Yin, *Talanta* **2019**, *200*, 432.
97. A. Yahia-Ammar, D. Sierra, F. Mérola, N. Hildebrandt, X. L. Guével, *ACS Nano* **2016**, *10*, 2591.
98. R. Vankayala, C. L. Kuo, K. Nuthalapati, C. S. Chiang, K. C. Hwang, *Adv. Funct. Mater.* **2015**, *25*, 5934.
99. J. Feng, P. Huang, F.-Y. Wu, *Analyst* **2017**, *142*, 4106.
100. M. Takahashi, T. Imaoka, Y. Hongo, K. Yamamoto, *Angew. Chem. Int. Ed.* **2013**, *52*, 7419.
101. W. Zhu, A. Noureddine, J. Y. Howe, J. Guo, C. J. Brinker, *Nano Lett*. **2019**, *19*, 1512.
102. M. A. Abbas, T.-Y. Kim, S. U. Lee, Y. S. Kang, J. H. Bang, *J. Am. Chem. Soc.* **2016**, *138*, 390.
103. A. Senthamizhan, A. Celebioglu, T. Uyar, *J. Mater. Chem. A* **2014**, *2*, 12717.
104. Y. Qiao, J. Shang, S. Li, L. Feng, Y. Jiang, Z. Duan, X. Lv, C. Zhang, T. Yao, Z. Dong, Y. Zhang, H. Wang, *Sci. Rep.* **2016**, *6*, 36494.
105. S. Saadi, B. Nazari, *J. Compos. Compd.* **2019**, *1*, 41.
106. T. Ameri, P. Khoram, J. Min, C. J. Brabec, *Adv. Mater.* **2013**, *25*, 4245.
107. R. Khan, M. H. Naveen, J. H. Bang, *ACS Energy Lett*. **2021**, *6*, 2713.
108. K. G. Stamplecoskie, G. Yousefalizadeh, L. Gozdzialski, H. Ramsay, *J. Phys. Chem. C* **2018**, *122*, 13738.
109. M. S. Kim, M. A. Abbas, J. H. Bang, *Bull. Korean Chem. Soc.* **2016**, *37*, 791.
110. M. A. Abbas, S. J. Yoon, R. Khan, J. Lee, J. H. Bang, *J. Phys. Chem. C* **2019**, *123*, 14921.
111. M. A. Abbas, S. J. Yoon, H. Kim, J. Lee, P. V. Kamat, J. H. Bang, *ACS Appl. Mater. Interfaces* **2019**, *11*, 12492.
112. H. Zhang, Z. Zhao, A. T. Turley, L. Wang, P. R. McGonigal, Y. Tu, Y. Li, Z. Wang, R. T. K. Kwok, J. W. Y. Lam, B. Z. Tang, *Adv. Mater.* **2020**, *32*, 2001457.
113. Z. Luo, X. Yuan, Y. Yu, Q. Zhang, D. T. Leong, J. Y. Lee, J. Xie, *J. Am. Chem. Soc.* **2012**, *134*, 16662.
114. Y. Yu, Z. Luo, D. M. Chevrier, D. T. Leong, P. Zhang, D.-e. Jiang, J. Xie, *J. Am. Chem. Soc.* **2014**, *136*, 1246.
115. Z. Wu, Q. Yao, O. J. H. Chai, N. Ding, W. Xu, S. Zang, J. Xie, *Angew. Chem. Int. Ed.* **2020**, *59*, 9934.
116. N. Shahzad, F. Chen, L. He, W. Li, H. Wang, *J. Power Sources* **2015**, *294*, 609.
117. W. Li, F. Chen, *J. Alloys Compd.* **2015**, *632*, 845.
118. N. Sakai, T. Ikeda, T. Teranishi, T. Tatsuma, *ChemPhysChem* **2011**, *12*, 2415.
119. M. Amjadi, K.-U. Kyung, I. Park, M. Sitti, *Adv. Funct. Mater.* **2016**, *26*, 1678.
120. J. Wang, C. Lu, K. Zhang, *Energy Environ. Mater.* **2020**, *3*, 80.
121. L. Tang, S. Wu, J. Qu, L. Gong, J. Tang, *Materials* **2020**, *13*, 3947.
122. A. Som, I. Chakraborty, T. A. Maark, S. Bhat, T. Pradeep, *Adv. Mater.* **2016**, *28*, 2827.
123. J. P. Xie, Y. G. Zheng, J. Y. Ying, *Chem. Commun.* **2010**, *46*, 961.
124. Y. Cai, L. Yan, G. Liu, H. Yuan, D. Xiao, *Biosens. Bioelectron.* **2013**, *41*, 875.
125. X. Liu, C. Zong, L. Lu, *Analyst* **2012**, *137*, 2406.
126. Y. Sun, J. Shao, H. Li, L. Cui, W. Ke, F. Zheng, Y. Zhao, *J. Photochem. Photobiol. A Chem.* **2019**, *374*, 68.
127. C. M. Hofmann, J. B. Essner, G. A. Baker, S. N. Baker, *Nanoscale* **2014**, *6*, 5425.
128. H. Ding, H. Li, P. Liu, J. K. Hiltunen, Y. Wu, Z. Chen, J. Shen, *Microchim. Acta* **2014**, *181*, 1029.
129. A. Senthamizhan, A. Celebioglu, B. Balusamy, T. Uyar, *Sci. Rep.* **2015**, *5*, 15608.
130. K. Chaiendoo, T. Tuntulani, W. Ngeontae, *Mater. Chem. Phys.* **2017**, *199*, 272.
131. S. Bothra, Y. Upadhyay, R. Kumar, S. K. Ashok Kumar, S. K. Sahoo, *Biosens. Bioelectron.* **2017**, *90*, 329.
132. H. Zhu, T. Yu, H. Xu, K. Zhang, H. Jiang, Z. Zhang, Z. Wang, S. Wang, *ACS Appl. Mater. Interfaces* **2014**, *6*, 21461.
133. Y.-X. Qi, M. Zhang, A. Zhu, G. Shi, *Analyst* **2015**, *140*, 5656.
134. S. Bothra, P. Paira, A. S. K. Kumar, R. Kumar, S. K. Sahoo, *ChemistrySelect* **2017**, *2*, 6023.
135. R.-X. Bian, X.-T. Wu, F. Chai, L. Li, L.-Y. Zhang, T.-T. Wang, C.-G. Wang, Z.-M. Su, *Sens. Actuators B Chem.* **2017**, *241*, 592.
136. F. Sang, X. Zhang, F. Shen, *Microchim. Acta* **2019**, *186*, 373.
137. M. S. Mathew, A. Baksi, T. Pradeep, K. Joseph, *Biosens. Bioelectron.* **2016**, *81*, 68.
138. H. Zhao, X. Wen, W. Li, Y. Li, C. Yin, *J. Mater. Chem. B* **2019**, *7*, 2169.
139. J. Nebu, J. S. Anjali Devi, R. S. Aparna, B. Aswathy, G. M. Lekha, G. Sony, *Anal. Bioanal. Chem.* **2019**, *411*, 997.
140. X. Wang, Z. Liu, W. Zhao, J. Sun, B. Qian, X. Wang, H. Zeng, D. Du, J. Duan, *Anal. Bioanal. Chem.* **2019**, *411*, 1009.
141. H. Li, M. Yang, D. Kong, R. Jin, X. Zhao, F. Liu, X. Yan, Y. Lin, G. Lu, *Sens. Actuators B Chem.* **2019**, *282*, 366.
142. K. Chatterjee, C. W. Kuo, A. Chen, P. Chen, *J. Nanobiotechnology* **2015**, *13*, 46.
143. X. Zhao, D. Kong, R. Jin, H. Li, X. Yan, F. Liu, P. Sun, Y. Gao, G. Lu, *Sens. Actuators B Chem.* **2019**, *296*, 126641.
144. X. Fang, Q. Zhao, H. Cao, J. Liu, M. Guan, J. Kong, *Analyst* **2015**, *140*, 7823.
145. S. Abarghoei, N. Fakhri, Y. S. Borghei, M. Hosseini, M. R. Ganjali, *Spectrochim. Acta A Mol. Biomol. Spectrosc.* **2019**, *210*, 251.
146. P. Zhang, Y. Wang, Y. Yin, *Sensors* **2016**, *16*, 1124.
147. L. Su, T. Shu, Z. Wang, J. Cheng, F. Xue, C. Li, X. Zhang, *Biosens. Bioelectron.* **2013**, *44*, 16.
148. A. Ghosh, V. Jeseentharani, M. A. Ganayee, R. G. Hemalatha, K. Chaudhari, C. Vijayan, T. Pradeep, *Anal. Chem.* **2014**, *86*, 10996.
149. B. L. Gregory, F. M. Smits, *IEEE Trans. Electron Devices* **1965**, *12*, 254.
150. E. Johnson, *RCA Rev.* **1973**, *34*, 80.
151. R. Parthasarathy, X.-M. Lin, H. M. Jaeger, *Phys. Rev. Lett.* **2001**, *87*, 186807.
152. C.-W. Jiang, I. C. Ni, S.-D. Tzeng, C.-S. Wu, W. Kuo, *Nanoscale* **2014**, *6*, 5887.
153. V. Aleksandrovic, D. Greshnykh, I. Randjelovic, A. Frömsdorf, A. Kornowski, S. V. Roth, C. Klinke, H. Weller, *ACS Nano* **2008**, *2*, 1123.
154. D. Greshnykh, A. Fromsdorf, H. Weller, C. Klinke, *Nano Lett*. **2009**, *9*, 473.
155. H. Lehmann, S. Willing, S. Möller, M. Volkmann, C. Klinke, *Nanoscale* **2016**, *8*, 14384.
156. Y. Cai, J. Michels, J. Bachmann, C. Klinke, *J. Appl. Phys.* **2013**, *114*, 034311.
157. S. Willing, H. Lehmann, M. Volkmann, C. Klinke, *Sci. Adv.* **2017**, *3*, e1603191.
158. H. Qian, M. Zhu, Z. Wu, R. Jin, *Acc. Chem. Res.* **2012**, *45*, 1470.
159. C. R. Kagan, C. B. Murray, *Nat. Nanotechnol.* **2015**, *10*, 1013.
160. D. V. Talapin, C. B. Murray, *Science* **2005**, *310*, 86.
161. L. Clarke, M. N. Wybourne, L. O. Brown, J. E. Hutchison, M. Yan, S. X. Cai, J. F. W. Keana, *Semicond. Sci. Technol.* **1998**, *13*, A111.
162. G. Schmid, Y.-P. Liu, M. Schumann, T. Raschke, C. Radehaus, *Nano Lett*. **2001**, *1*, 405.
163. P. Yuan, R. Zhang, E. Selenius, P. Ruan, Y. Yao, Y. Zhou, S. Malola, H. Häkkinen, B. K. Teo, Y. Cao, N. Zheng, *Nat. Commun.* **2020**, *11*, 2229.
164. H. Jiang, W. Hu, *Angew. Chem. Int. Ed.* **2020**, *59*, 1408.
165. E. Talgorn, R. D. Abellon, P. J. Kooyman, J. Piris, T. J. Savenije, A. Goossens, A. J. Houtepen, L. D. A. Siebbeles, *ACS Nano* **2010**, *4*, 1723.
166. L. Bozano, B. Kean, V. Deline, J. Salem, J. Scott, *Appl. Phys. Lett.* **2004**, *84*, 607.

167. N. Hirata, M. Sato, E. Tsunemi, Y. Watanabe, H. Tsunoyama, M. Nakaya, T. Eguchi, Y. Negishi, A. Nakajima, *J. Phys. Chem. C* **2017**, *121*, 10638.
168. T. Yokoyama, N. Hirata, H. Tsunoyama, Y. Negishi, A. Nakajima, *AIP Adv.* **2018**, *8*, 065002.
169. B. Kim, H. Seong, J. T. Song, K. Kwak, H. Song, Y. C. Tan, G. Park, D. Lee, J. Oh, *ACS Energy Lett*. **2020**, *5*, 749.
170. H.-H. Deng, Q.-Q. Zhuang, K.-Y. Huang, P. Balasubramanian, Z. Lin, H.-P. Peng, X.-H. Xia, W. Chen, *Nanoscale* **2020**, *12*, 15791.
171. Z. Wang, B. Chen, A. S. Susha, W. Wang, C. J. Reckmeier, R. Chen, H. Zhong, A. L. Rogach, *Adv. Sci.* **2016**, *3*, 1600182.
172. Z. Wang, B. Chen, M. Zhu, S. V. Kershaw, C. Zhi, H. Zhong, A. L. Rogach, *ACS Appl. Mater. Interfaces* **2016**, *8*, 33993.
173. Z. Wang, A. S. Susha, B. Chen, C. Reckmeier, O. Tomanec, R. Zboril, H. Zhong, A. L. Rogach, *Nanoscale* **2016**, *8*, 7197.
174. Q. Huang, M.-Y. Hu, Y.-L. Li, N. Chen, L. Yi, Q.-h. Wei, F. Fu, *Chem. Commun.* **2021**.*57*, 9890. https://doi.org/10.1039/D1CC03799D.
175. E. Khatun, S. Bose, M. Jash, T. Pradeep, *J. Chem. Sci.* **2018**, *130*, 147.
176. S. K. Mishra, S. Raveendran, J. Ferreira, S. Kannan, *Langmuir* **2016**, *32*, 10305.
177. N. C. Jeong, H.-J. Son, C. Prasittichai, C. Y. Lee, R. A. Jensen, O. K. Farha, J. T. Hupp, *J. Am. Chem. Soc.* **2012**, *134*, 19820.
178. T. Chen, Q. Yao, R. R. Nasaruddin, J. Xie, *Angew. Chem. Int. Ed.* **2019**, *58*, 11967.
179. Q. Yao, X. Yuan, V. Fung, Y. Yu, D. T. Leong, D.-e. Jiang, J. Xie, *Nat. Commun.* **2017**, *8*, 927.
180. Q. Yao, V. Fung, C. Sun, S. Huang, T. Chen, D.-E. Jiang, J. Y. Lee, J. Xie, *Nat. Commun.* **2018**, *9*, 1979.
181. T. Chen, V. Fung, Q. Yao, Z. Luo, D.-E. Jiang, J. Xie, *J. Am. Chem. Soc.* **2018**, *140*, 11370.
182. C. Wang, H. Dong, L. Jiang, W. Hu, *Chem. Soc. Rev.* **2018**, *47*, 422.

AUTHOR BIOGRAPHIES

Lizhen Chen received her BS degree in Applied Chemistry from Xiangtan University, China, in 2012 and her MS degree in Analytical Chemistry from Changchun Institute of Applied Chemistry, Chinese Academy of Sciences and University of Chinese Academy of Sciences, China, in 2015. After that, she joined the R&D team, Foxconn, China, to develop metallic surficial nanopores for electronic products. Since September 2018, she has been pursuing her PhD degree under the co-supervision of Dr. Indranath Chakraborty and Prof. Dr. Wolfgang J. Parak at University of Hamburg, Germany. Her current research focuses on the design and synthesis of metal nanoclusters for catalyst and biology applications.

Christian Klinke studied physics at the University of Würzburg and the University of Karlsruhe (Germany). After he obtained his PhD from the EPFL in Lausanne (Switzerland), he worked as post-doc at the IBM T. J. Watson Research Center in Yorktown Heights (USA). Returning to Germany, he started an assistant professorship at the University of Hamburg. His research was supported by an ERC Starting Grant and a Heisenberg fellowship of the German Funding Agency DFG. Following that period, he became an associate professor at the Swansea University. Since 2019, he is also full professor at the University of Rostock in Germany. His research concerns the colloidal synthesis of nanomaterials and the optoelectronic characterization of these materials.

Indranath Chakraborty obtained his Ph.D. in chemistry from the Indian Institute of Technology, Madras (India). He was then a postdoctoral research associate at the University of Illinois at Urbana–Champaign, IL, USA. Later, he was an Alexander von Humboldt Postdoctoral Research Fellow at Philipps University of Marburg, Germany. Currently, he is a research associate at the Center for Hybrid Nanostructure, University of Hamburg, Germany. His research area primarily focused on synthesis of atomically precise nanoclusters and emerging properties of these materials.

How to cite this article: L. Chen, A. Black, W. J. Parak, C. Klinke, I. Chakraborty, *Aggregate* **2022**, *3*, e132. https://doi.org/10.1002/agt2.132